2017 Fall

"Phase Transformation *in* Materials"

12.04.2017

Eun Soo Park

Office: 33-313
Telephone: 880-7221
Email: espark@snu.ac.kr
Office hours: by an appointment

Contents for previous class

< Phase Transformation in Solids >

1) Diffusional Transformation

(a) Precipitation

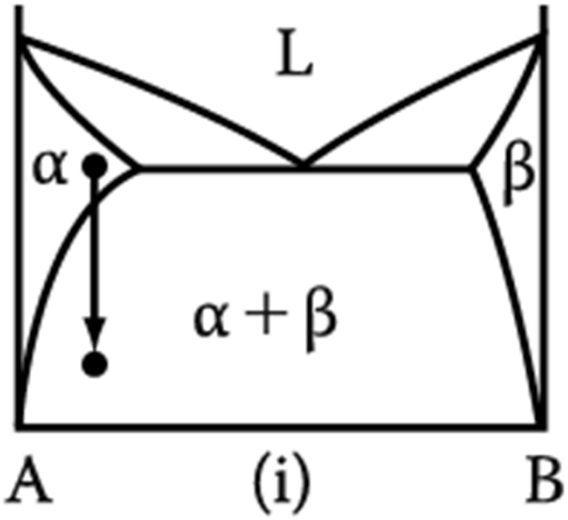

Homogeneous Nucleation

➡ Effect of misfit strain energy

$$\Delta G = -V\Delta G_V + A\gamma + V\Delta G_S$$

$$r^* = \frac{2\gamma}{(\Delta G_V - \Delta G_S)} \qquad \Delta G^* = \frac{16\pi\gamma^3}{3(\Delta G_V - \Delta G_S)^2}$$

$$N_{\text{hom}} = \omega C_0 \exp\left(-\frac{\Delta G_m}{kT}\right)\exp\left(-\frac{\Delta G^*}{kT}\right)$$

Heterogeneous Nucleation

➡ suitable nucleation sites ~ nonequilibrium defects

(creation of nucleus~destruction of a defect($-\Delta G_d$))

$$\Delta G_{het} = -V(\Delta G_V - \Delta G_S) + A\gamma - \Delta G_d$$

$$\frac{\Delta G^*_{het}}{\Delta G^*_{\text{hom}}} = \frac{V^*_{het}}{V^*_{\text{hom}}} = S(\theta)$$

$$\frac{N_{het}}{N_{\text{hom}}} = \frac{C_1}{C_0}\exp\left(\frac{\Delta G^*_{\text{hom}} - \Delta G^*_{het}}{kT}\right)$$

Rate of Homogeneous Nucleation Varies with undercooling below T_e for alloy X_0

Effective equilibrium temperature is reduced by misfit strain E term, ΔGs.

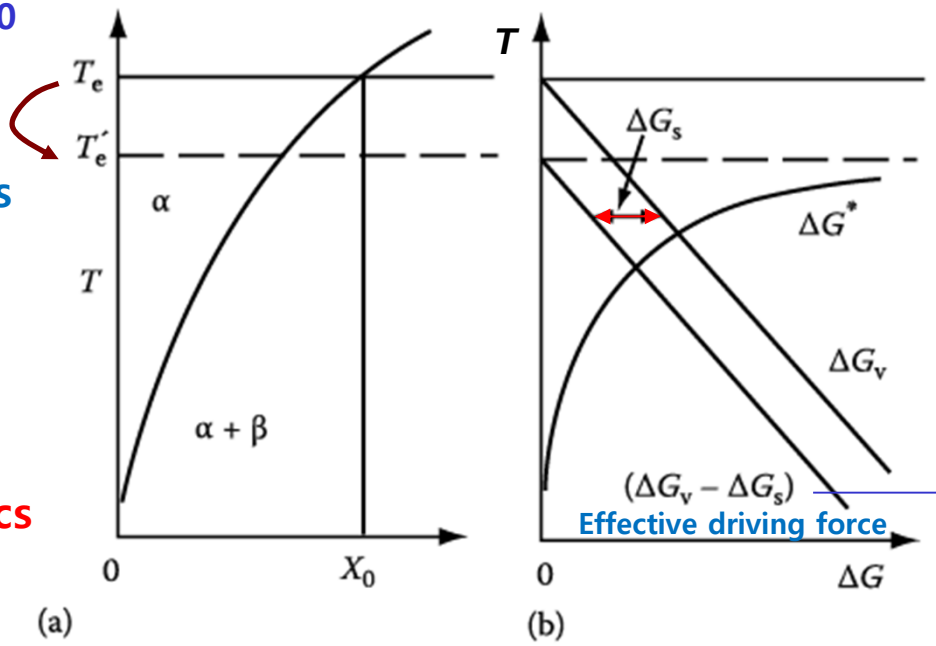

$$\Delta G_V \propto \Delta X \propto \Delta T$$

Composition dependent

$$\Delta G^* = \frac{16\pi\gamma^3}{3(\Delta G_V - \Delta G_S)^2}$$

Resultant energy barrier for nucleation

Thermodynamics

vs

Kinetics

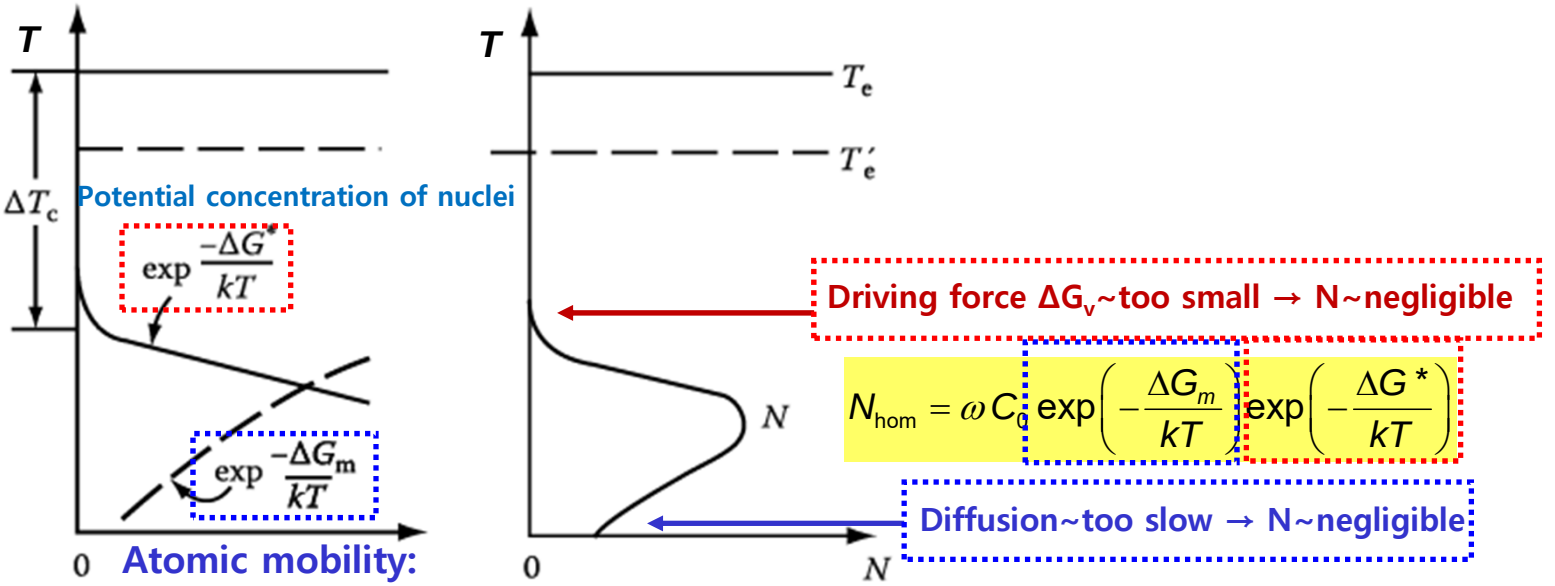

Driving force ΔG_v~too small → N~negligible

$$N_{hom} = \omega C_0 \exp\left(-\frac{\Delta G_m}{kT}\right) \exp\left(-\frac{\Delta G^*}{kT}\right)$$

Diffusion~too slow → N~negligible

- **Precipitate growth**

1) Growth behind Planar Incoherent Interfaces

Diffusion-Controlled Thickening:

$$x \propto \sqrt{(Dt)}$$ Parabolic growth

$$v = \frac{D(\Delta C_0)^2}{2(C_\beta - C_e)(C_\beta - C_0)x}$$

$$v \propto \Delta X_0 \propto \sqrt{(D/t)}$$

Supersaturation

2) Diffusion Controlled lengthening of Plates or Needles

Diffusion Controlled lengthening:

$$v = \frac{D\Delta X_0}{k(X_\beta - X_r)} \cdot \frac{1}{r}\left(1 - \frac{r^*}{r}\right)$$

r ↑ ⟶ ΔX ↑

$v \rightarrow$ constant ⟶ $x \propto t$

Linear growth

3) Thickening of Plate-like Precipitates

Thickening of Plate-like Precipitates by Ledge Mechanism

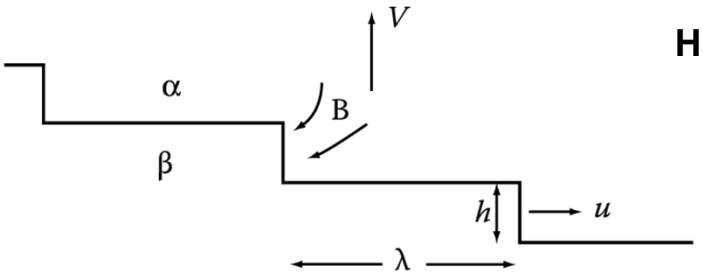

Half Thickness Increase

$$v = \frac{uh}{\lambda} \longrightarrow v = \frac{D\Delta X_0}{k(X_\beta - X_e)\lambda}$$

u : rate of lateral migration

5.4 Overall Transformation Kinetics

If isothermal transformation,

The fraction of Transformation as a function of Time and Temp. → f (t,T)

TTT Diagram ⟺ CCT Diagram

* Constant Nucleation Rate Conditions

$$f(t) = 1 - \exp\left(-f_e(t)\right) = 1 - \exp\left(-\frac{\pi}{3} I v^3 t^4\right)$$

* Short time:
1-exp(z)~Z (z ≪1)

* Long time:
t→∞, f →1

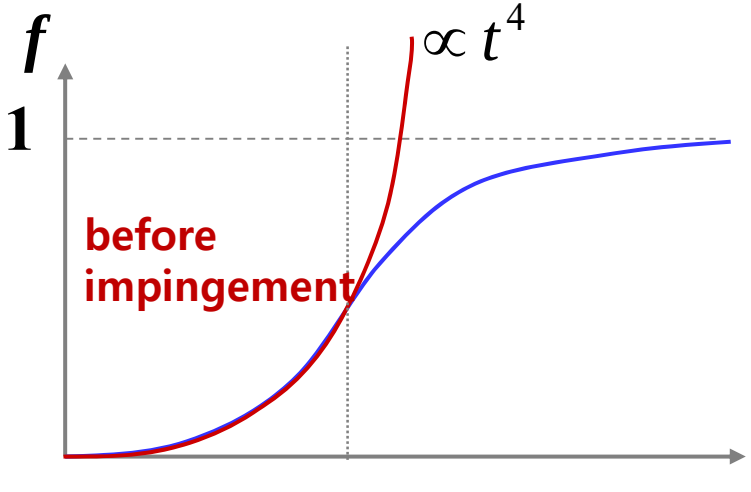

Johnson-Mehl-Avrami Equation

$$f = 1 - \exp\left(-kt^n\right)$$

$-\frac{\pi}{3} I v^3$

k: *T* sensitive ***f*(*I*, *v*)**

n: **1 ~ 4 (depend on nucleation mecnanism)**

Growth controlled. **Nucleation-controlled.**

If no change of nucleation mechanism during phase transformation, n is not related to T.

i.e. 50% transform

Exp (-0.7) = 0.5

$$kt_{0.5}^n = 0.7 \qquad t_{0.5} = \frac{0.7}{k^{1/n}} \xrightarrow{\frac{\pi}{3} I v^3} t_{0.5} = \frac{0.9}{I^{1/4} v^{3/4}}$$

Rapid transformations are associated with (large values of k), or (rapid nucleation and growth rates)

Time–Temperature–Transformation Curves (TTT)

- How much time does it take at any one temperature for a given fraction of the liquid to transform (nucleate and grow) into a crystal?

- $f(t,T) \sim \pi I(T) \mu(T)^3 t^4/3$

  where f is the fractional volume of crystals formed, typically taken to be 10^{-6}, a barely observable crystal volume.

Nucleation rates

$$I = n\nu \exp\left\{\left(\frac{16\pi\Delta H_{cryst}}{81RT}\right)\left(\frac{T_m}{\Delta T}\right)^2\right\}\exp\left\{\frac{-\Delta E_D}{RT}\right\}$$

Growth rates

$$\mu(T) = \left(\frac{fRT}{3N\pi a^2 \eta(T)}\right)\left(1-\exp\left[\left(\frac{\Delta H_m}{RT}\right)\left(\frac{\Delta T}{T_m}\right)\right]\right)$$

* Time-Temperature-Transformation diagrams

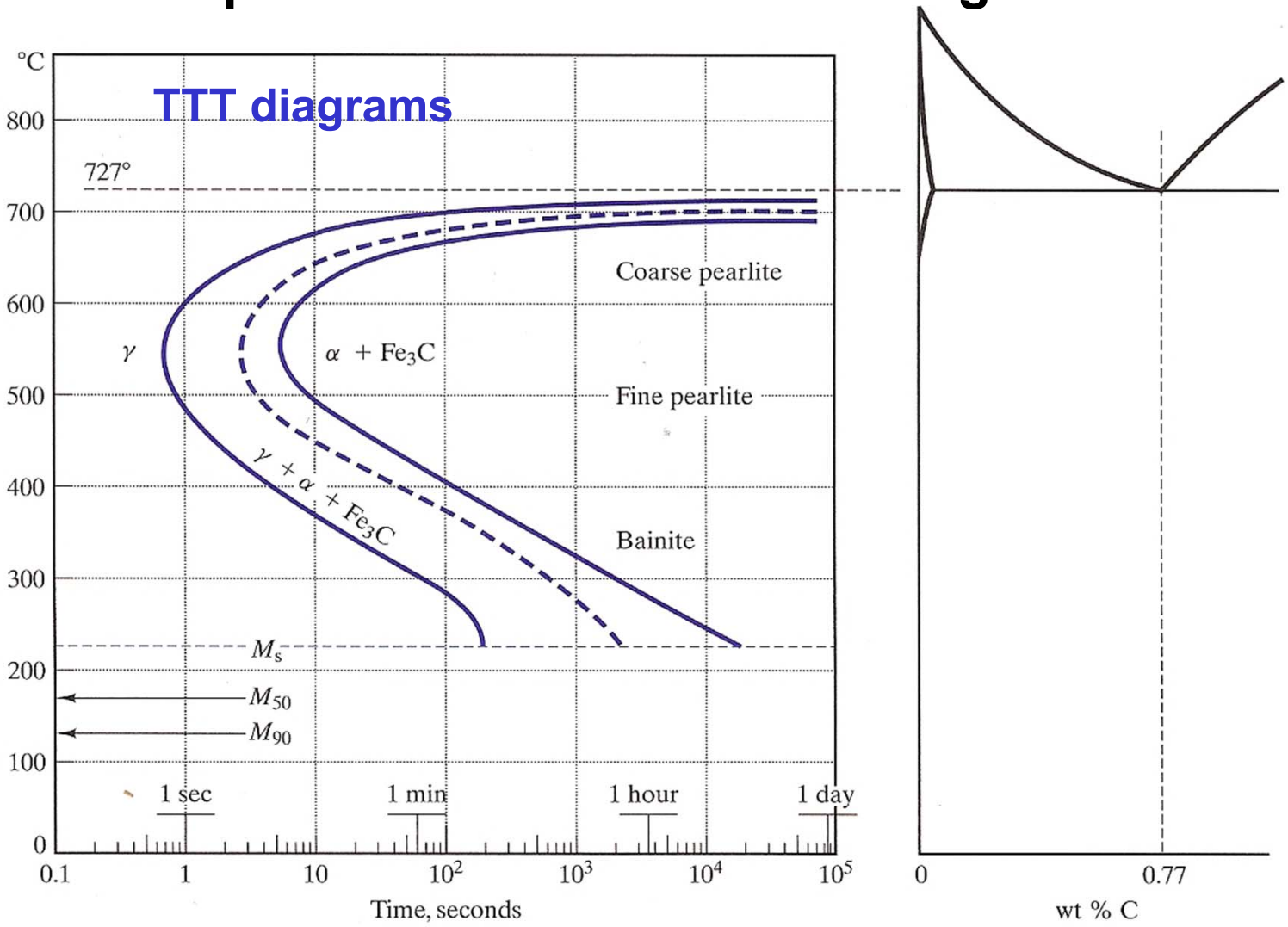

FIGURE 10.11 *A more complete TTT diagram for eutectoid steel than was given in Figure 10.7. The various stages of the time-independent (or diffusionless) martensitic transformation are shown as horizontal lines. M_s represents the start, M_{50} represents 50% transformation, and M_{90} represents 90% transformation. One hundred percent transformation to martensite is not complete until a final temperature (M_f) of −46°C.*

* Continuous Cooling Transformation diagrams

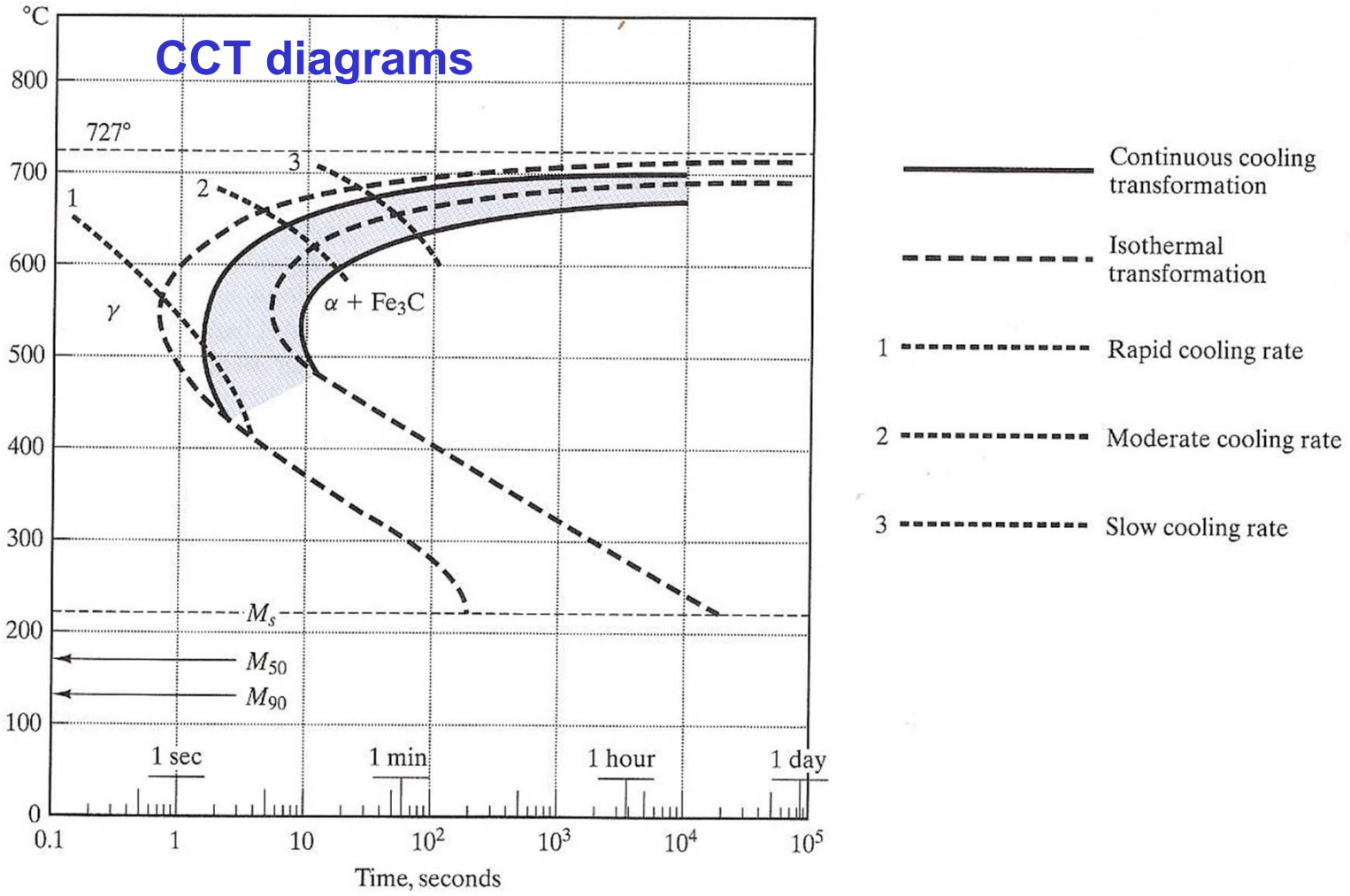

FIGURE 10.14 *A continuous cooling transformation (CCT) diagram is shown superimposed on the isothermal transformation diagram of Figure 10.11. The general effect of continuous cooling is to shift the transformation curves downward and toward the right. (After* Atlas of Isothermal Transformation and Cooling Transformation Diagrams, *American Society for Metals, Metals Park, OH, 1977.)*

Let us now turn to a consideration of some examples of the great variety of civilian transformations in solid.

5.5 Precipitation in Age-Hardening Alloys

Precipitation in Aluminum-Copper Alloys

Al-4 wt%Cu (1.7 at %)

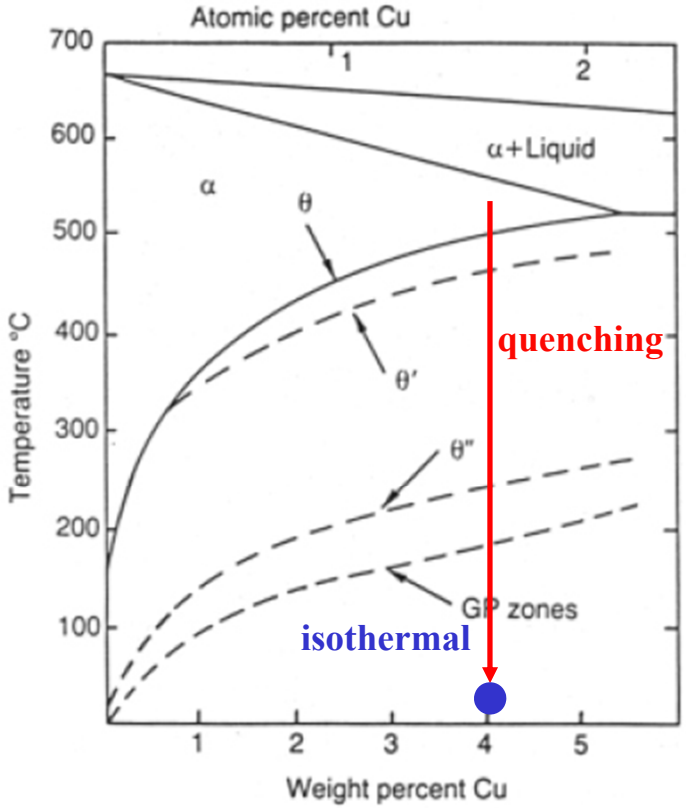

α_0 **540°C heat treatment →**
Quenching + Isothermal (below 180°C)

Supersaturated solid solution

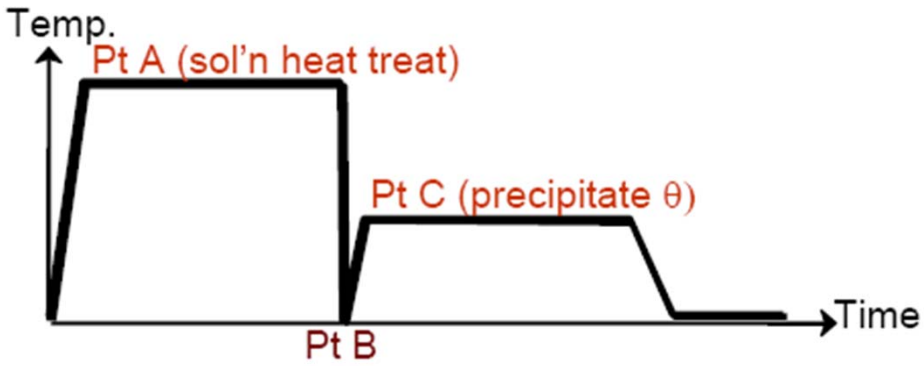

→ α_1+GP zones

→α_2+θ″ →α_3+θ′ →α_4+θ

($CuAl_2$)

Fig. 5.25 Al-Cu phase diagram showing the metastable GP zone, Θ″ and Θ′ solvuses. (Reproduced from G. Lorimer, *Precipitation Processes in Solids*, K.C. Russell and H.I. Aaronson (Eds.), The Metallurgical Society of AMIE, 1978, p. 87.)

In most system, α, β phase~ different crystal structure → incoherent nuclei with large γ ~ impossible to homogeneous nucleation of β → Homogeneous nucleation of metastable phase β′ (GP Zones, Section 5.5.1)

Transition phases

$\alpha_0 \rightarrow \alpha_1$+GP zone$\rightarrow \alpha_2$+$\theta''$ $\rightarrow \alpha_3$+θ' $\rightarrow \alpha_4$+θ ($CuAl_2$)

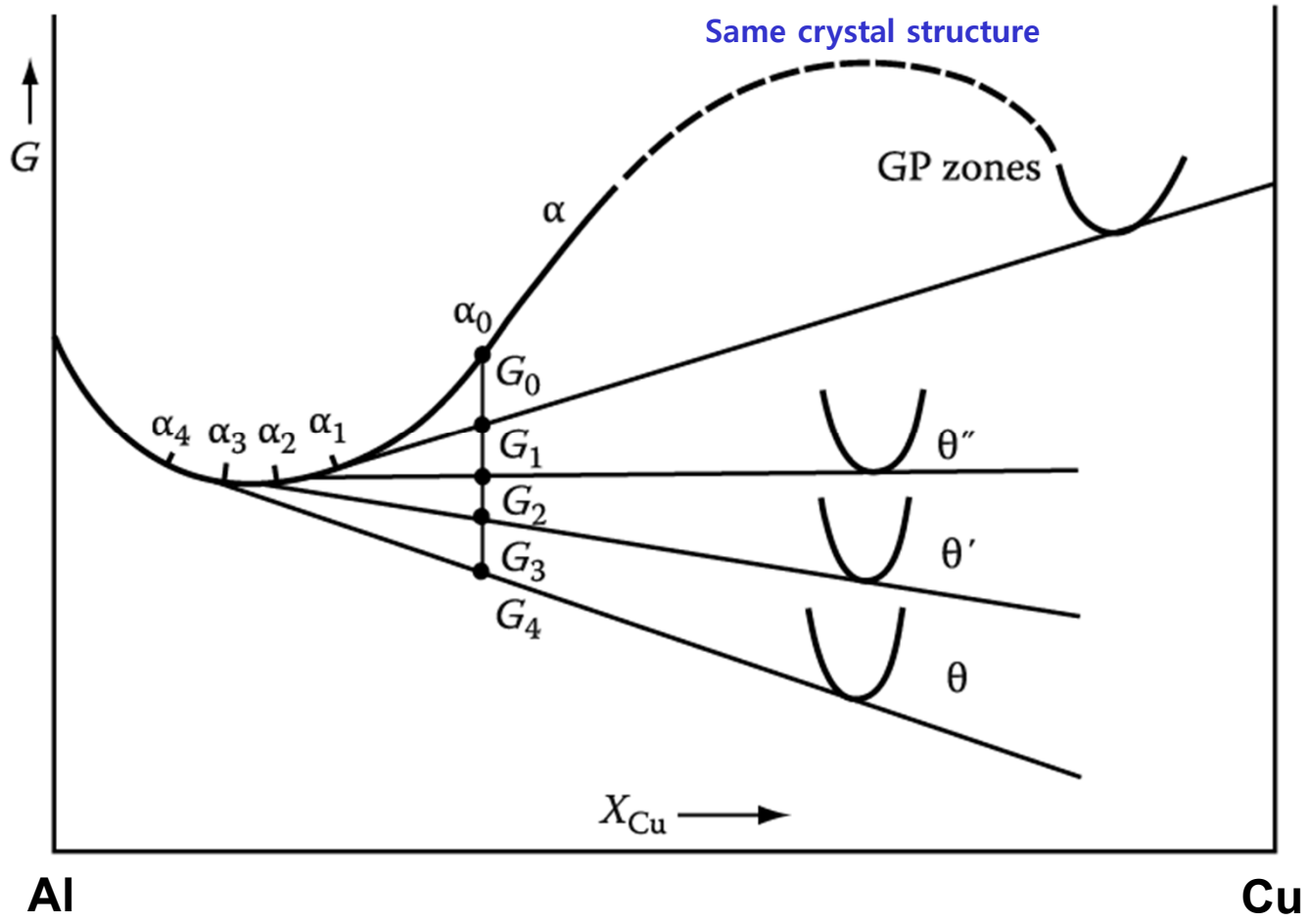

Fig. 5.27 A schematic molar free energy diagram for the Al-Cu system.

The Crystal Structures of θ″, θ′ and θ

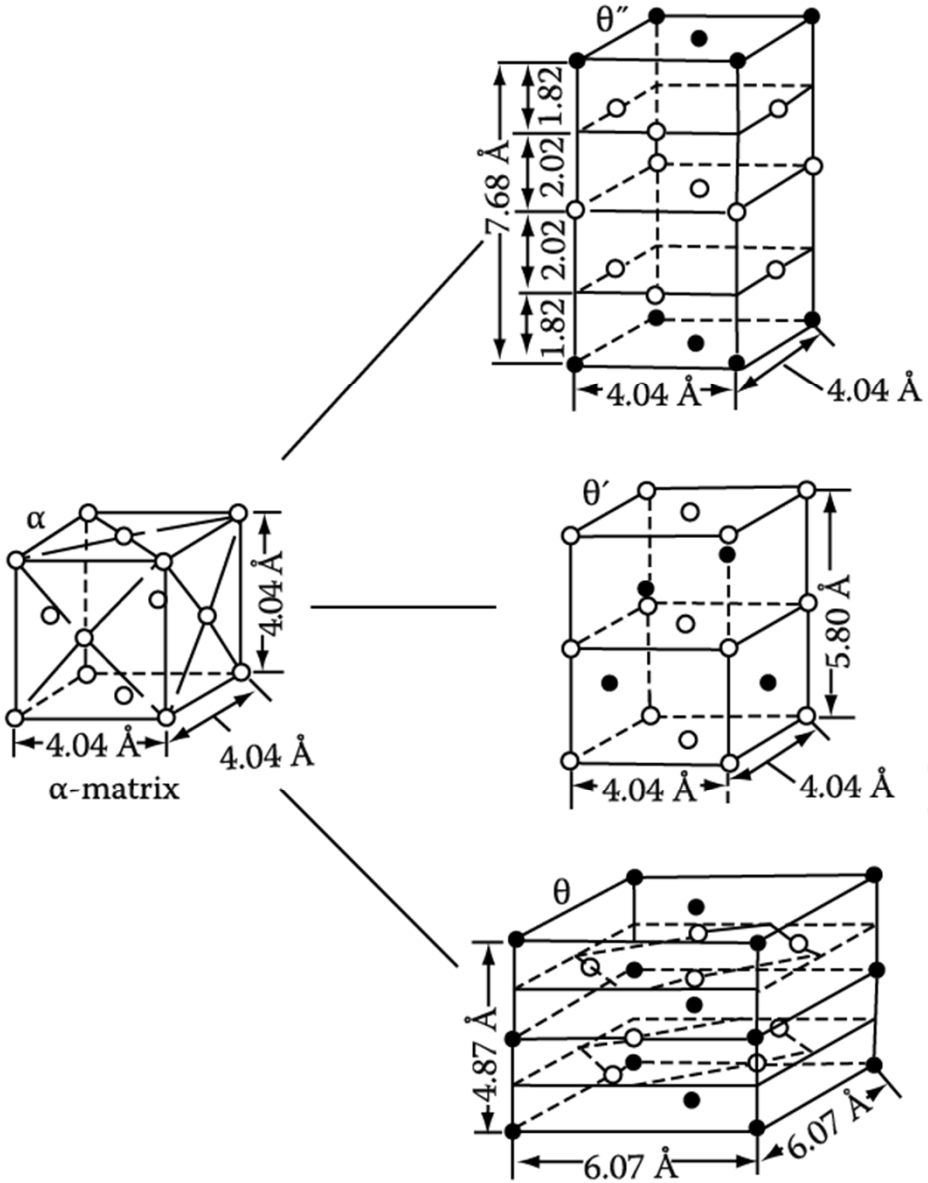

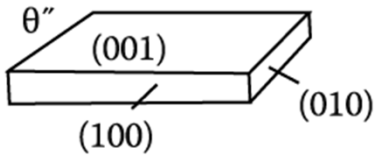

All sides coherent

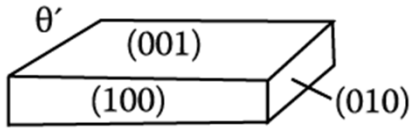

(001) Coherent or semicoherent

(100) } Not coherent
(010) }

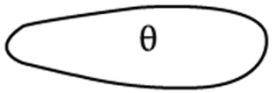

Incoherent

A tetragonal unit cell (= a distorted fcc structure in which the Cu and Al atoms are ordered on (001) planes.)

& a small distortion in the [001] direction of (010) and (100) faces

A tetragonal with an approximate composition $CuAl_2$

Different crystal structure in (010) and (100) faces to the matrix and a large misfit in the [001] direction

Approximate composition $CuAl_2$ and complex BCT structure

Fig. 5.29 Structure and morphology of θ'', θ' and θ in Al-Cu (○ Al. ● Cu).

$\alpha_0 \rightarrow \alpha_1$+GP zone$\rightarrow\alpha_2+\theta'' \rightarrow\alpha_3+\theta' \rightarrow\alpha_4+\theta$ ($CuAl_2$)

Low Activation Energy of Transition Phases

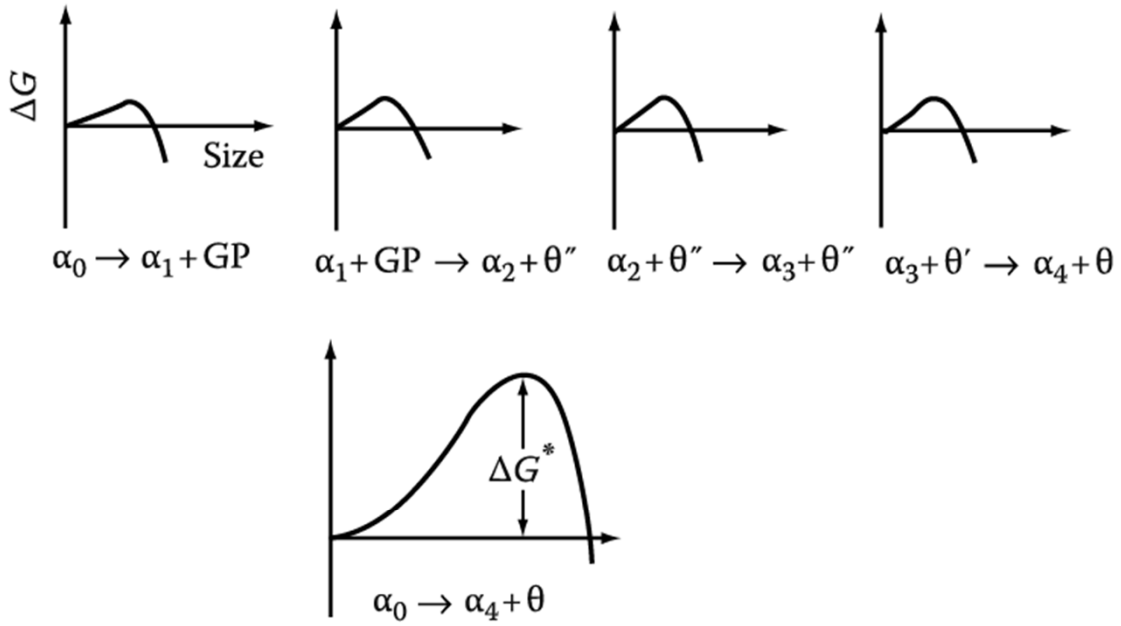

∵ the crystal structures of the transition phases are intermediate between those of the matrix and the equilibrium phase.

Transition phases (중간상, θ″ & θ′): a high degree of coherence, low interfacial E contribution to min ΔG*.

Equilibrium phase (평형상, θ): complex crystal structure that is incompatible with the matrix → high E interfaces and high ΔG*.

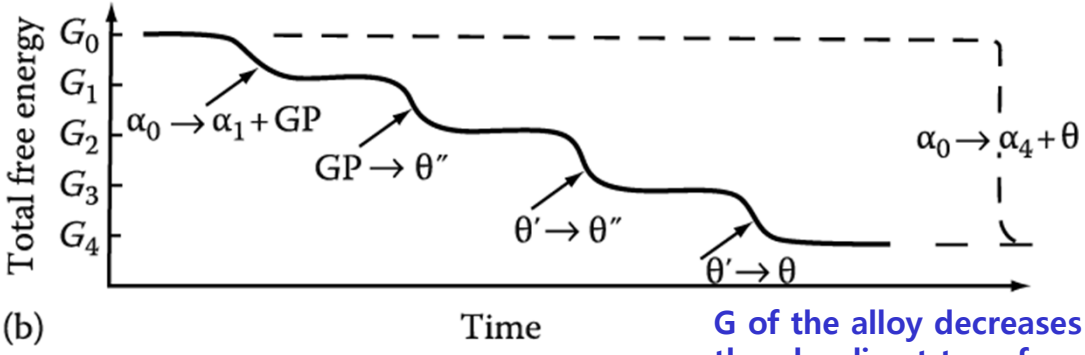

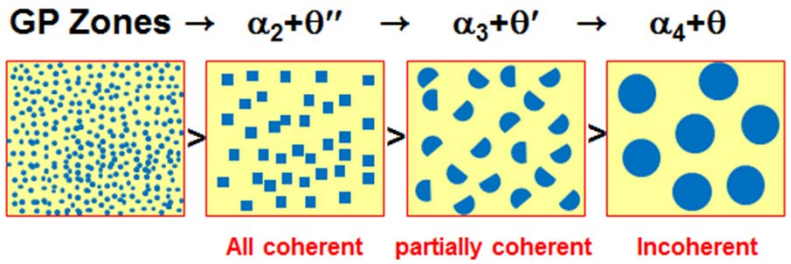

G of the alloy decreases more rapidly via the transition phases than by direct transformation to the equilibrium phase.

(a) The activation E barrier to the formation of each transition phase is very small in comparison to the barrier against the direct precipitation of the equilibrium phase. (b) Schematic diagram showing the total free E of the alloy versus time.

* Effect of Aging Temperature on the Sequence of Precipitates

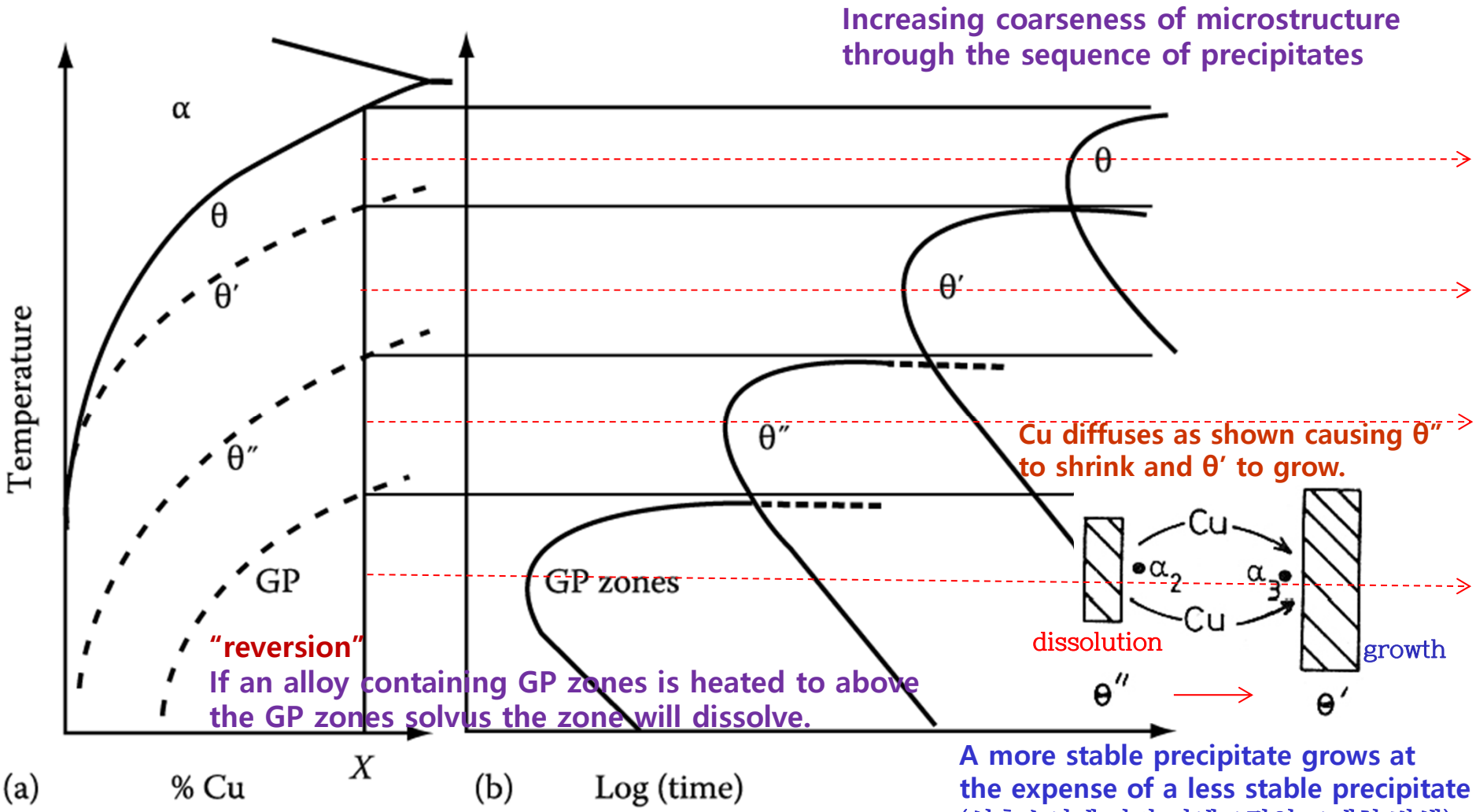

Fig. 5.32 (a) Metastable solvus lines in Al-Cu (schematic).
(b) Time for start of precipitation at different temperatures for alloy X in (a).

5.5.4. Age Hardening

Transition phase precipitation → great improvement in the mechanical properties

Coherent precipitates→highly strained matrix→the main resistance to the Ⓓ movement: solid solution hardening

Hardness vs. Time by Ageing

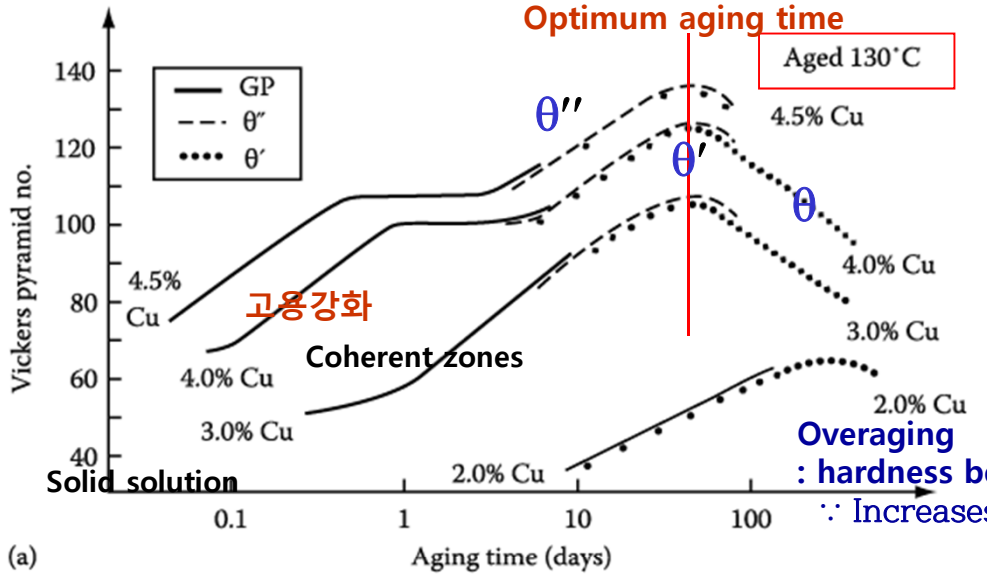

Maximum hardness~ largest fraction of θ″ (coherent precipitates)

Ageing at 130°C produces higher maximum hardness than ageing at 190°C.

At 130°C, however, it takes too a long time (several tens of days).

∵ Increases the distance btw precipitates making Ⓓ bowing easier

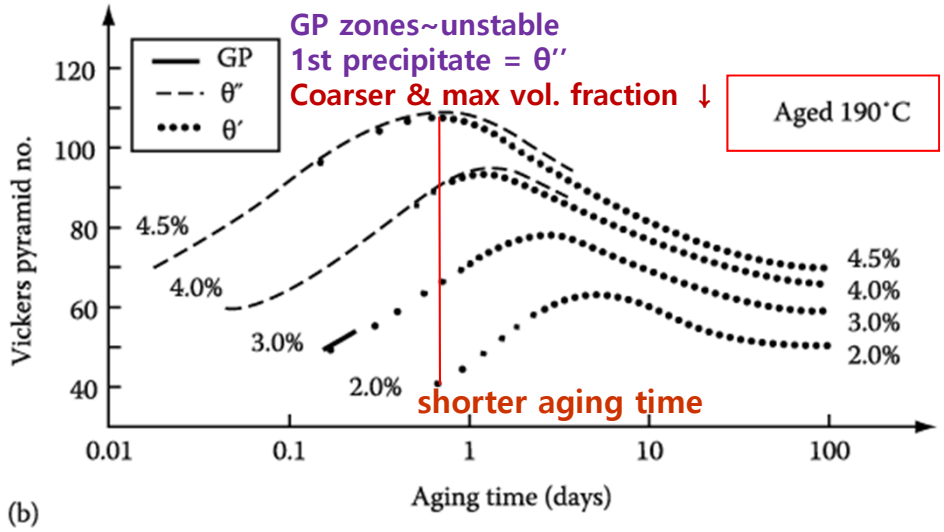

How can you get the high hardness for the relatively short ageing time (up to 24h)?

Double ageing treatment

first below the GP zone solvus → fine dispersion of GP zones then ageing at higher T.

: Engineering alloys are not heat treated for max. strength alone. → **to optimize other properties**

best heat treatment in practice

Fig. 5. 37 Hardness vs. time for various Al-Cu alloys at (a) 130 ℃ (b) 190 ℃

The theory of nucleation and growth can provide general guidelines for understanding civilian transformation.

5.5 Precipitation in Age-Hardening Alloys

Table 5.2 Some precipitation-Hardening Sequences

Base Metal	Alloy	Precipitation Sequence
Aluminum	Al–Ag	GPZ (spheres) $\rightarrow \gamma'$ (plates) $\rightarrow \gamma$ (Ag_2Al)
	Al–Cu	GPZ (disks) $\rightarrow \theta''$ (disks) $\rightarrow \theta'$ (plates) $\rightarrow \theta$ ($CuAl_2$)
	Al–Cu–Mg	GPZ (rods) $\rightarrow S'$ (laths) $\rightarrow S$ ($CuMgAl_2$) (laths)
	Al–Zn–Mg	GPZ (spheres) $\rightarrow \eta'$ (plates) $\rightarrow \eta$ ($MgZn_2$) (plates or rods)
	Al–Mg–Si	GPZ (rods) $\rightarrow \beta'$ (rods) $\rightarrow \beta$ (Mg_2Si) (plates)
Copper	Cu–Be	GPZ (disks) $\rightarrow \gamma' \rightarrow \gamma$ (CuBe)
	Cu–Co	GPZ (spheres) $\rightarrow \beta$ (Co) (plates)
Iron	Fe–C	ε-carbide (disks) $\rightarrow Fe_3C$ (plates)
	Fe–N	α'' (disks) $\rightarrow Fe_4N$
Nickel	Ni–Cr–Ti–Al	γ' (cubes or spheres)

Source: Mainly from Martin, J.W., in *Precipitation Hardening*, Pergamon Press, Oxford, 1968.

Q3: Quenched-in vacancies vs Precipitate-free zone

5.5.3. Quenched-in Vacancies

If $X_v < X_v^c$ critical vacancy supersaturation,
Precipitate nucleation X → formation of PFZ

In the vicinity of grain boundaries on subsequent aging,

a) Excess Ⓥ→ Ⓓ nucleation and moving ↑:
Heterogeneous nucleation sites ↑
b) Excess Ⓥ → atomic mobility ↑ at ageing temp:
speeds up the process of nucleation and growth
ex) rapid formation of GP zones at the relatively low aging temperature. (possible to RT aging in Al-Cu alloy)

a) Precipitate-Free Zone(PFZ) due to Vacancy Diffusion during quenching

Solute concentration within the zone ~ largely unchanged, but no precipitate at GB
∵ a critical vacancy supersaturation must be exceeded for nucleation to occur.

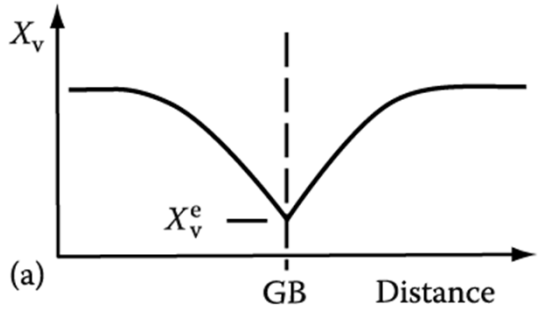

Similar PFZs can also form at inclusions and dislocations.

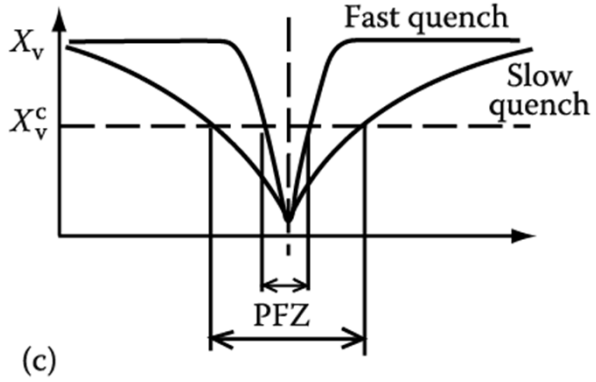

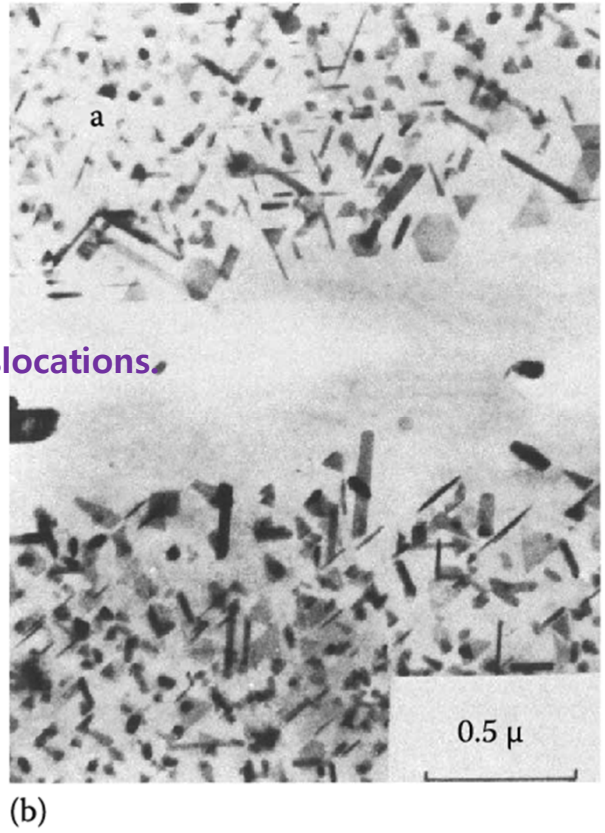

Fig. 5.35 A PFZ due to vacancy diffusion to a grain boundary during quenching.
(a) Vacancy concentration profile. (b) A PFZ in an Al-Ge alloy (x 20,000)
(c) Dependence of PFZ width on critical vacancy concentration X_v^c and rate of quenching.

* Equilibrium Vacancy Concentration

at equilibrium $\left(\frac{dG}{dX_V}\right)_{X_V = X_V^e} = 0$

$$\Delta H_V - T\Delta S_V + RT \ln X_V^e = 0$$

A constant ~3, independent of T

Rapidly increases with increasing T

$$X_V^e = \exp\frac{\Delta S_V}{R} \cdot \exp\frac{-\Delta H_V}{RT}$$

putting $\Delta G_V = \Delta H_V - T\Delta S_V$

$$X_V^e = \exp\frac{-\Delta G_V}{RT}$$

increases exponentially with increasing T

- **In practice, ΔH_V is of the order of 1 eV per atom and X_V^e reaches a value of about 10^{-4}~10^{-3} at the melting point of the solid**

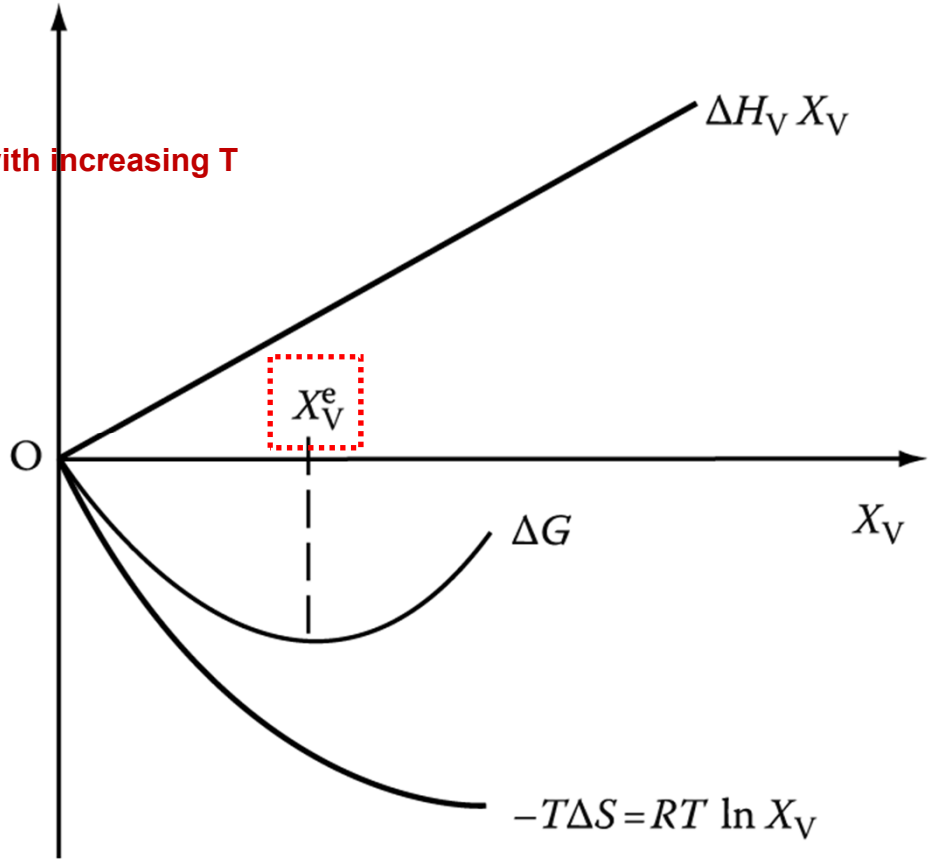

Fig. 1.37 Equilibrium vacancy concentration.

: adjust so as to reduce G to a minimum

b) Another cause of PFZs can be the nucleation and growth of GB precipitates during cooling from the solution treatment temperature.

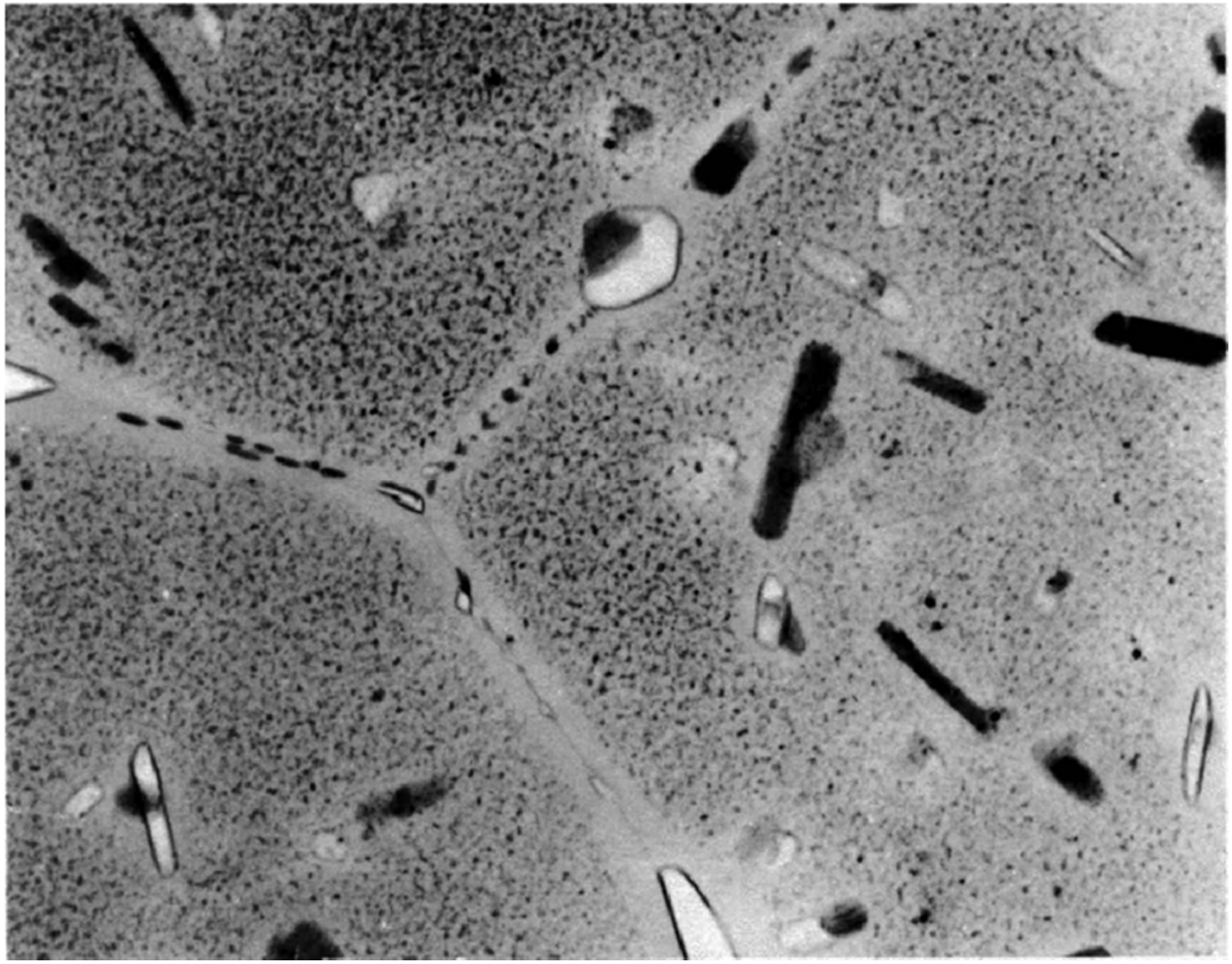

Fig. 5.36 PFZs around grain boundaries in a high-strength commercial Al-Zn-Mg-Cu alloy. Precipitates on grain boundaries have extracted solute from surrounding matrix. (x 59,200)

Q5: Spinodal Decomposition

5.5.5 Spinodal Decomposition

Spinodal mode of transformation has no barrier to nucleation

: describing the transformation of a system of two or more components in a metastable phase into two stable phases

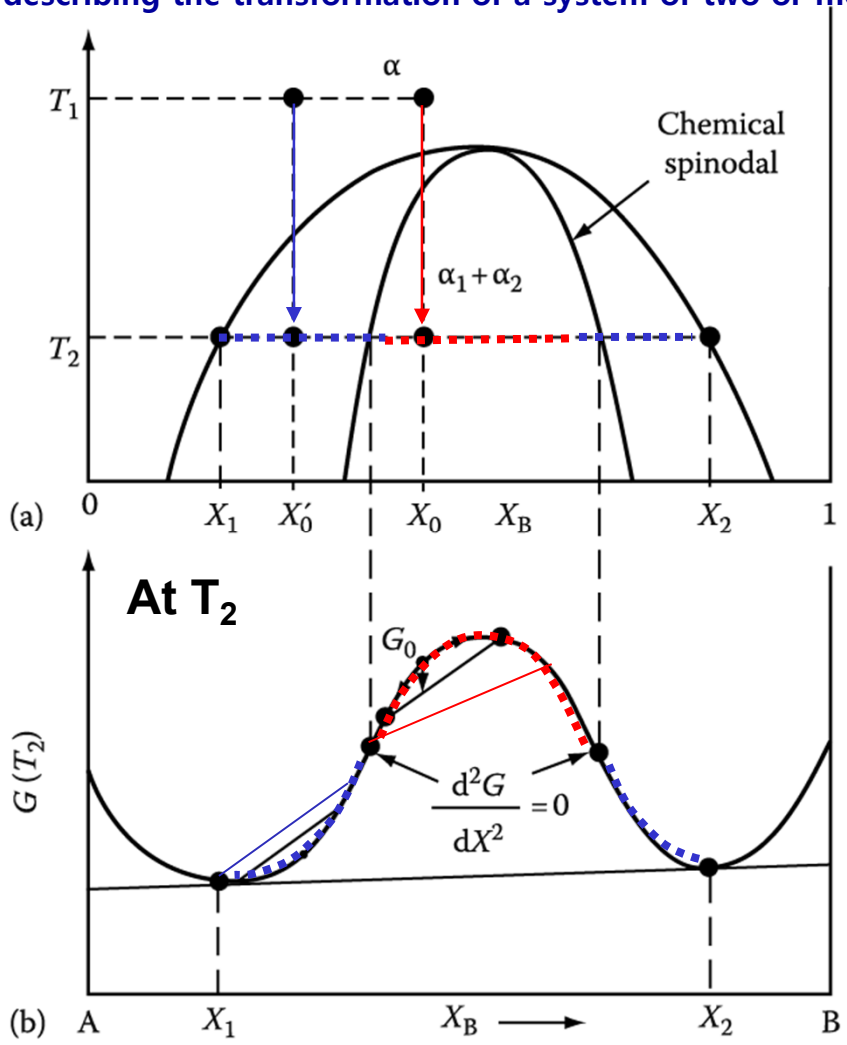

Fig. 5.38 Alloys between the spinodal points are unstable and can decompose into two coherent phasees α_1 and α_2 without overcoming an activation energy barrier. Alloys between the coherent miscibility gaps and the spinodal are metastable and can decompose only after nucleation of the other phase.

How does it differ between inside and outside the inflection point of Gibbs free energy curve?

1) Within the spinodal $\frac{d^2G}{dX^2}<0$

: phase separation by small fluctuations in composition/ "up-hill diffusion"

2) If the alloy lies outside the spinodal, small variation in composition leads to an increase in free energy and the alloy is therefore metastable.

The free energy can only be decreased if nuclei are formed with a composition very different from the matrix.

→ **nucleation and growth**
: "down-hill diffusion"

a) Composition fluctuations within the spinodal

b) Normal down-hill diffusion outside the spinodal

up-hill diffusion

down-hill diffusion

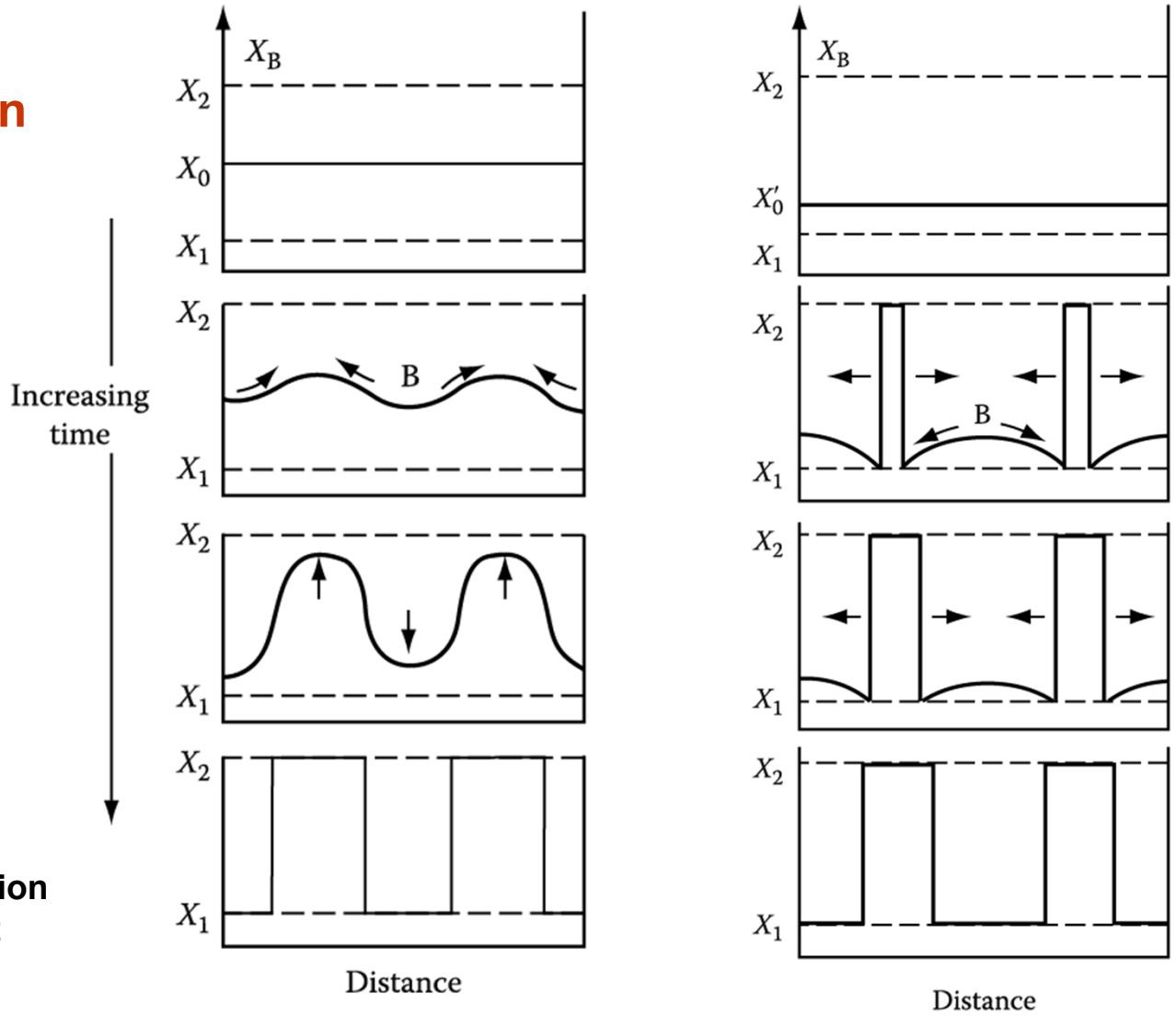

interdiffusion coefficient D<0

Fig. 5.39 & 5.40 schematic composition profiles at increasing times in (a) an alloy quenched into the spinodal region (X_0 in Figure 5.38) and (b) an alloy outside the spinodal points (X_0' in Figure 5.38)

Phase separation

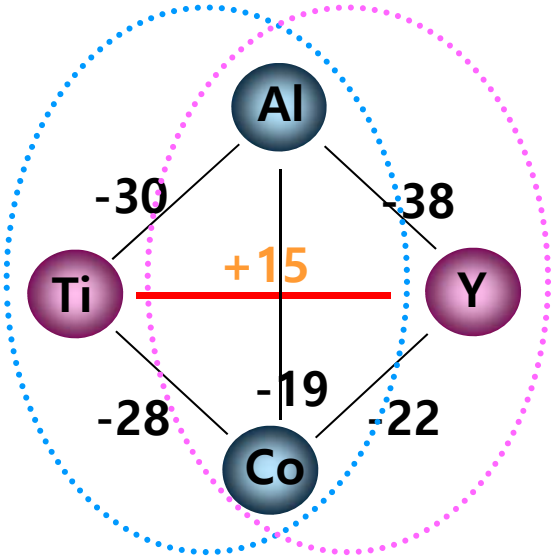

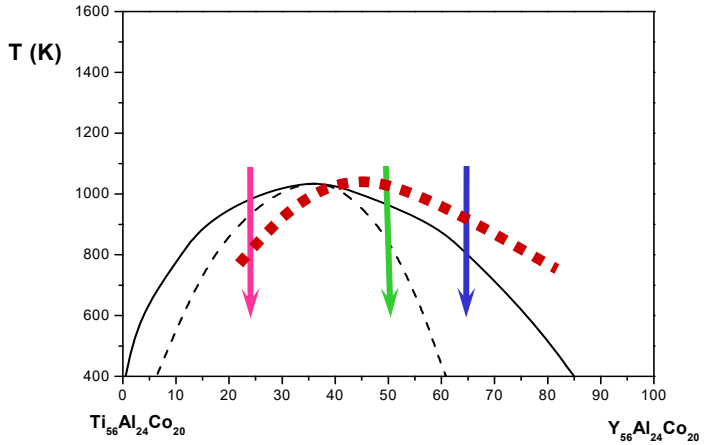

Droplet structure

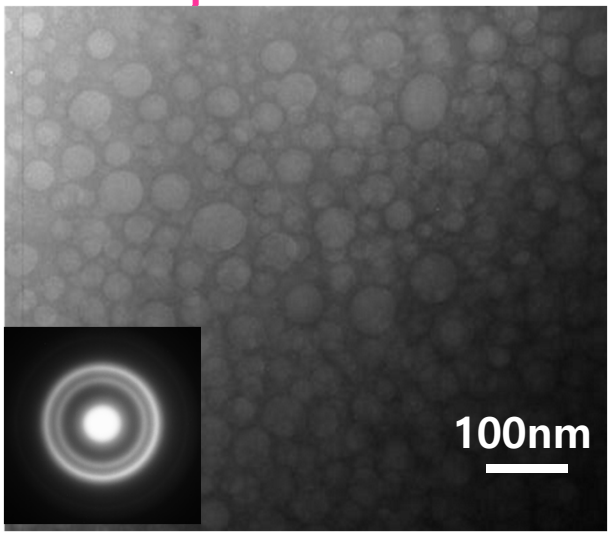

$(Y_{56}Al_{24}Co_{20})_{25}(Ti_{56}Al_{24}Co_{20})_{75}$

Interconnected structure

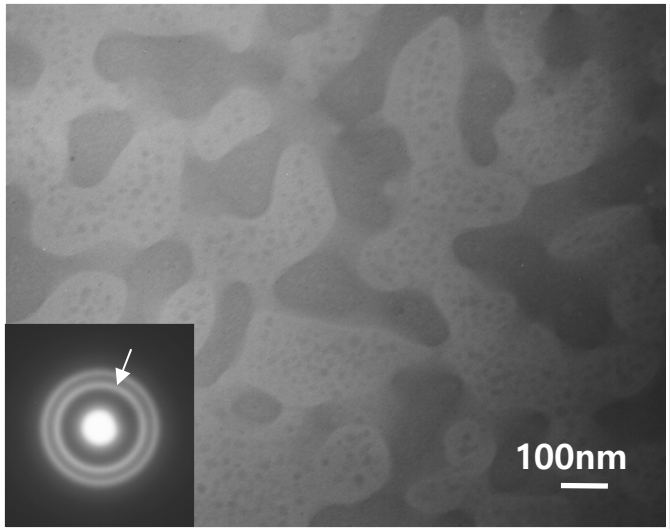

$(Y_{56}Al_{24}Co_{20})_{50}(Ti_{56}Al_{24}Co_{20})_{50}$

Droplet structure

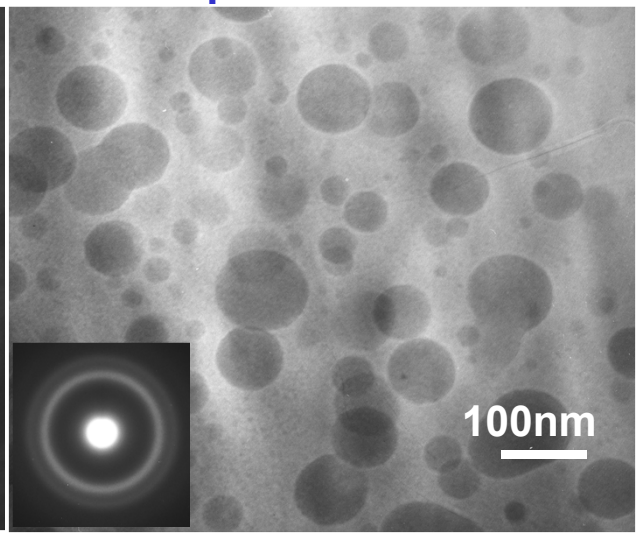

$(Y_{56}Al_{24}Co_{20})_{65}(Ti_{56}Al_{24}Co_{20})_{35}$

5.5.5 Spinodal Decomposition

* The Rate of Spinodal decomposition

a) Rate controlled by interdiffusion coefficient D (상호확산계수)

Within the spinodal D < 0,

composition fluctuation $\propto \exp(-t/\tau)$

(next page)

$$\tau = -\lambda^2 / 4\pi^2 D$$

τ: characteristic time constant

λ: wavelength of the composition modulations

(assumed one-dimensional)

b) Kinetics depends on λ: Transformation rate ↑ as λ ↓ (as small as possible).

But, minimum value of λ below which spinodal decomposition cannot occur.

Solutions to the diffusion equations

Ex1. Homogenization of sinusoidal varying composition in the elimination of segregation in casting

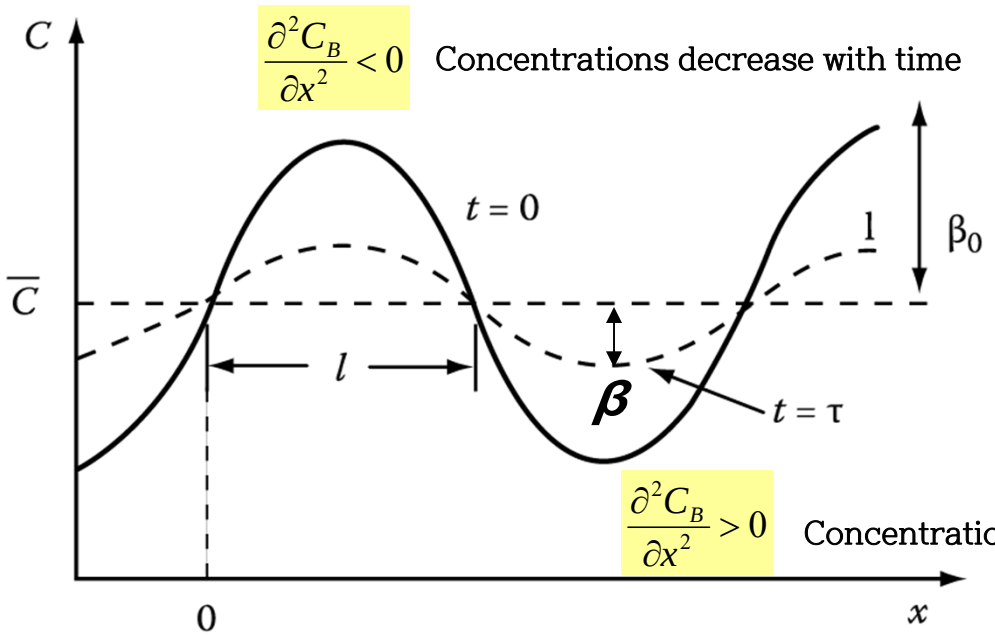

Fig. 2.10 The effect of diffusion on a sinusoidal variation of composition.

$$C = \overline{C} + \beta_0 \sin\frac{\pi x}{l} \quad \text{at t=0}$$

$$C = \overline{C} + \beta_0 \sin\frac{\pi x}{l}\exp\left(\frac{-t}{\tau}\right)$$

$$\beta = \beta_0 \exp(-t/\tau) \quad at \quad x = \frac{l}{2}$$

Amplitude of the concentration profile (β) decreases exponentially with time, $C \Rightarrow \overline{C}$

$$\tau = \frac{l^2}{\pi^2 D}$$

τ : relaxation time

"decide homogenization rate"

The initial concentration profile will not usually be sinusoidal, but in general any concentration profile can be considered as the sum of an infinite series of sine waves of varying wavelength and amplitude, and each wave decays at a rate determined by its own "τ". Thus, the short wavelength terms die away very rapidly and the homogenization will ultimately be determined by τ for the longest wavelength component.

* **Calculation of the wavelength (λ) of the composition fluctuations**

→ **Free Energy change for the decomposition**

1) Decomposition of X_0 into $X_0 + \Delta X$ and $X_0 - \Delta X$

What would be an additional energy affecting spinodal decomposition?

In practice, it is necessary to consider two important factors

2) interfacial energy

3) coherency strain energy

1) Decomposition of X_0 into $X_0 + \Delta X$ and $X_0 - \Delta X$

$$\Delta G_{chem} = \frac{1}{2}\frac{d^2G}{dX^2}(\Delta X)^2$$

Gibb's free energy reduction by compositional change

$$f(a+h) = f(a) + f'(a)h + \frac{f''(a)}{2!}h^2 + \cdots$$

$$G(X_0 + \Delta X) \approx G(X_0) + G'(X_0)\Delta X + \frac{G''(X_0)}{2!}\Delta X^2$$

$$G(X_0 - \Delta X) \approx G(X_0) - G'(X_0)\Delta X + \frac{G''(X_0)}{2!}\Delta X^2$$

$$\Delta G_{chem} = \frac{G(X_0 + \Delta X) + G(X_0 - \Delta X)}{2} - G(X_0)$$

$$= \frac{G''(X_0)}{2!}\Delta X^2 = \frac{1}{2}\frac{d^2G}{dX^2}\Delta X^2$$

5.5.5 Spinodal Decomposition

2) During the early stages, the interface between A-rich and B-rich region is not sharp but very diffuse. → diffuse interface

ΔG by formation of interface btw decomposed phases

Interfacial Energy
(gradient energy)

∝ composition gradient across the interface
: increased # of unlike nearest neighbors in a solution containing composition gradients

$$\Delta G_\gamma = K\left(\frac{\Delta X}{\lambda}\right)^2$$

Max. compositional gradient ΔX/λ

K : a proportionality constant dependent on the difference in the bond energies of like and unlike atom pair

If the size of the atoms making up the solid solution are different, the generation of composition differences, ΔX will introduce a coherency strain energy term, ΔGs.

3) Coherency Strain Energy
(atomic size difference)

$$\Delta G_S \propto E\delta^2 \Leftarrow \delta = (da/dX)\,\Delta X/a$$

δ: misfit between the A-rich & B-rich regions, E: Young's modulus, a: lattice parameter

$$\Delta G_S = \eta^2(\Delta X)^2 E' V_m$$

$$\text{where } \eta = \frac{1}{a}\left(\frac{da}{dX}\right), E' = E/(1-\nu)$$

ΔGs~ independent of λ

η: the fractional change in lattice parameter per unit composition change

*** Total free E change by the formation of a composition fluctuation 1) + 2) + 3)**

$$\Delta G = \left\{\frac{d^2G}{dX^2} + \frac{2K}{\lambda^2} + 2\eta^2 E' V_m\right\}\frac{(\Delta X)^2}{2}$$

5.5.5 Spinodal Decomposition

* Total free E change by the formation of a composition fluctuation

$$\Delta G = \left\{ \frac{d^2G}{dX^2} + \frac{2K}{\lambda^2} + 2\eta^2 E' V_m \right\} \frac{(\Delta X)^2}{2} < 0$$

a) Condition for Spinodal Decomposition

(→ a homogeneous solid solution~unstable)

$$-\frac{d^2G}{dX^2} > \frac{2K}{\lambda^2} + 2\eta^2 E' V_m$$

b) The Limit of T and composition in coherent spinodal decomposition

(스피노달 분해가 일어나는 온도와 조성의 한계값)

$$\lambda \to \infty$$

$$\frac{d^2G}{dX^2} = -2\eta^2 E' V_m$$

→ **coherent spinodal**

It lies entirely within the chemical spinodal ($d^2G/dX^2=0$)

(boundary btw ③ & ④, next page)

Wavelength for coherent spinodal

$$\lambda^2 > -2K \Big/ \left(\frac{d^2G}{dX^2} + 2\eta^2 E' V_m \right)$$

→ The minimum possible wavelength (λ) decreases with increasing undercooling (ΔT~ΔX) below the coherent spinodal.

This figure include the lines defining the equilibrium compositions of the coherent/ incoherent phases that result from spinodal decomposition.

* Incoherent(or equilibrium) miscibility gap: $\Delta H > 0$

The miscibility gap the normally appears on an equilibrium phase is the incoherent (or equilibrium) miscibility gap.→ equilibrium compositions of incoherent phases without strain fields.

a) **chemical spinodal: $d^2G/dX^2=0$_no practical importance X**

b) **Area ② , ΔG_V-ΔG_S < 0 → only incoherent strain-free nuclei can form.**

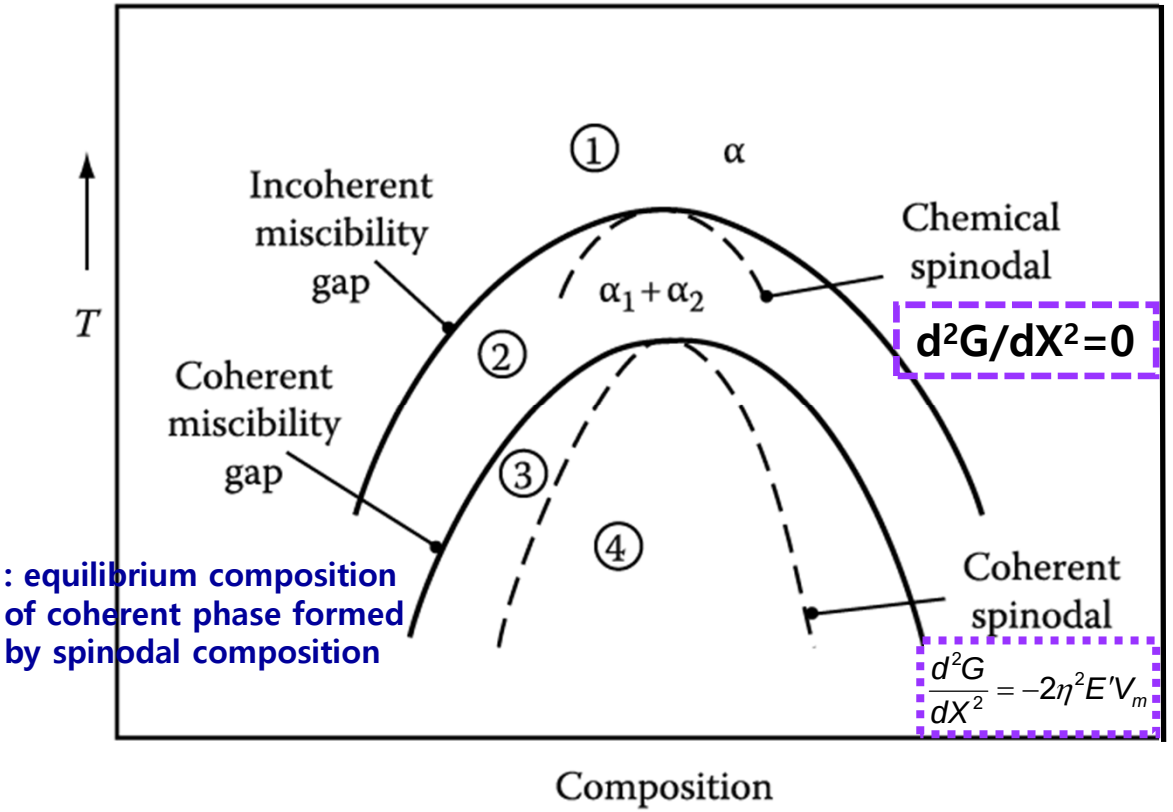

Figure 5.41 Schematic phase diagram for a clustering system.

Region 1: homogeneous α stable. Region 2: homogeneous α metastable, only incoherent phases can nucleate. Region 3: homogeneous α metastable, coherent phase can nucleate. Region 4: homogeneous α unstable, no nucleation barrier, spinodal decomposition occurs.

Spinodal decomposition is not only limited to systems containing a stable miscibility gap

All systems in which *GP zones* form, for example, containing a metastable coherent miscibility gap, i.e., the GP zone solvus.

→ at high supersaturation, GP zone can form by the spinodal mechanism.

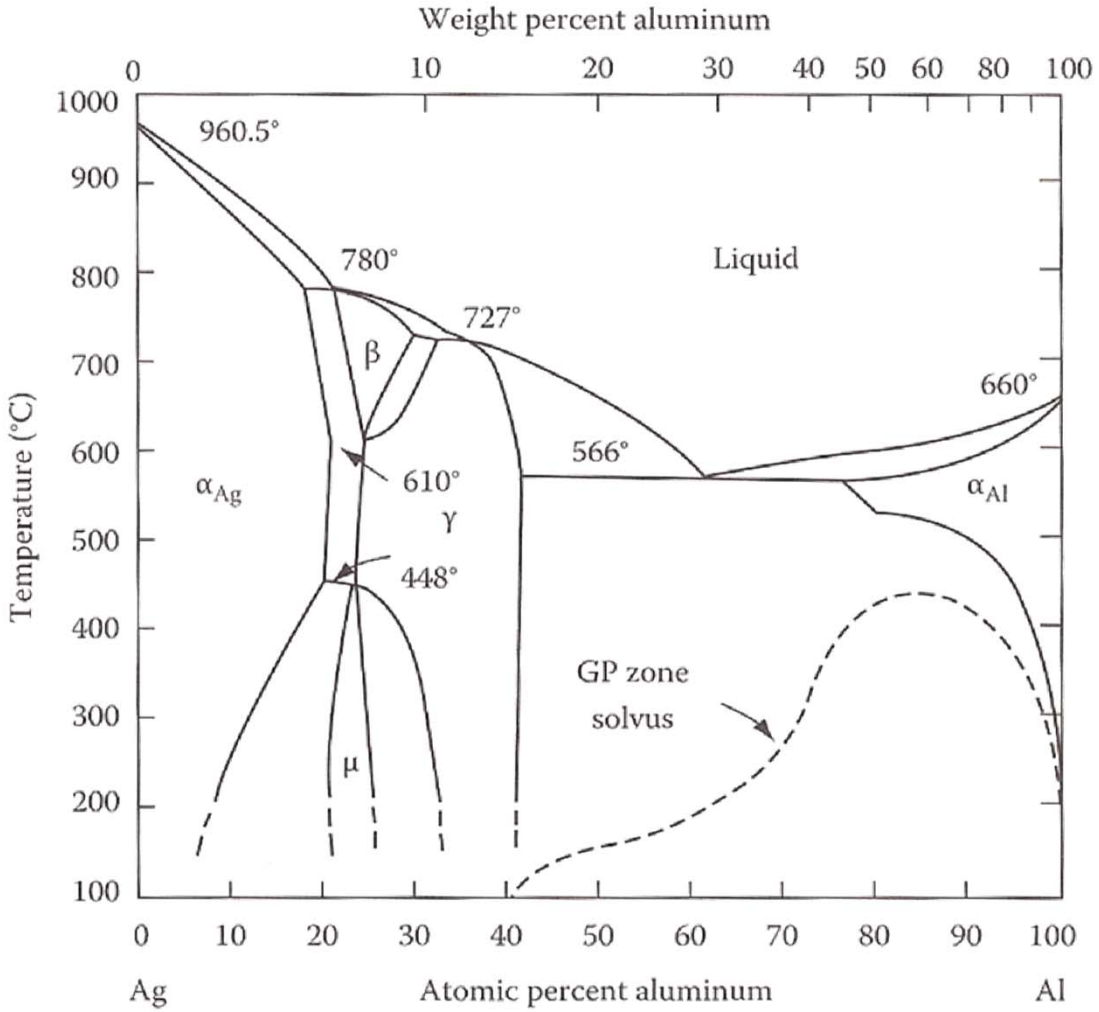

Figure 5.34

Al-Ag phase diagram showing metastable two-phase field corresponding to GP zones.

- The difference in T between the coherent and incoherent miscibility gaps, or the chemical and coherent spinodals $\propto$ **magnitude of** $|\eta|$ η: the fractional change in lattice parameter per unit composition change
- Large atomic size difference → $|\eta|$ **large**→large undercooling to overcome the strain E effects
- Like Al-Cu, large values of $|\eta|$ in cubic metals can be mitigated if the misfit strains are accommodated in the elastically soft <100> directions. → composition modulations building up normal to {100}

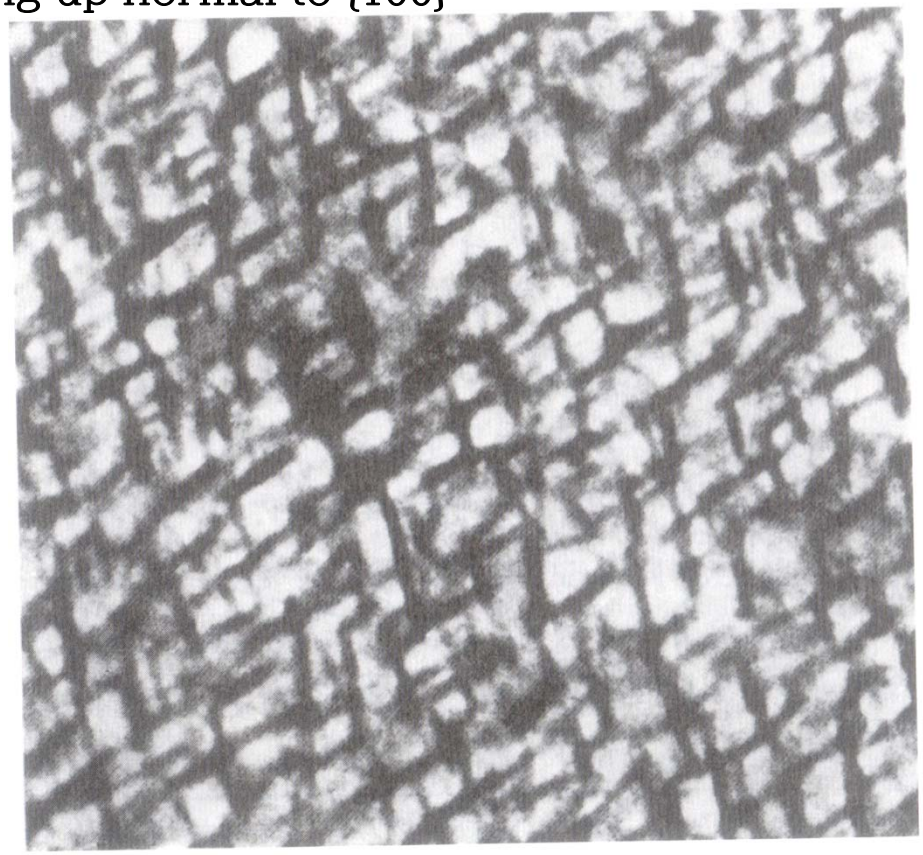

Figure 5.42 A coarsened spinodal microstructure in Al-22.5 Zn-0.1 Mg (at%) solution treated 2h at 400 ℃ and aged 20h at 100℃. Thin foil electron micrograph. λ = 25 nm_coarsening

Q6: How can you design an alloy with high strength at high T?

Microstructure of a two phase alloy is always unstable if the total interfacial free E is not a minimum. →

5.5.6. Particle Coarsening (smaller total interfacial area→loss of strength or disappearance of GB pining effect→ particular concern in the design of materials for high temp. applications)

Two Adjacent Spherical Precipitates with Different Diameters

(Gibbs-Thomson effect: radius of curvature↓ → X_B ↑)

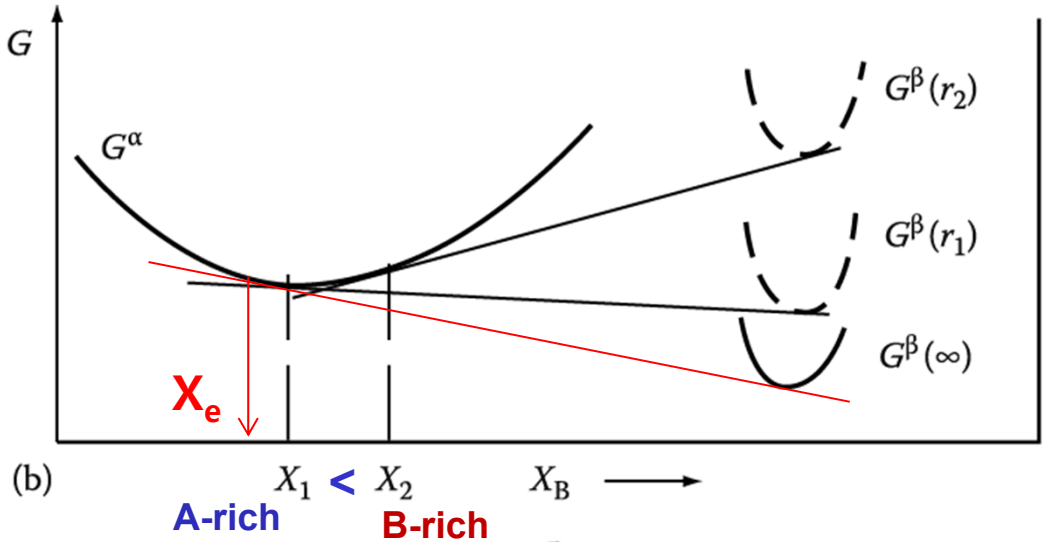

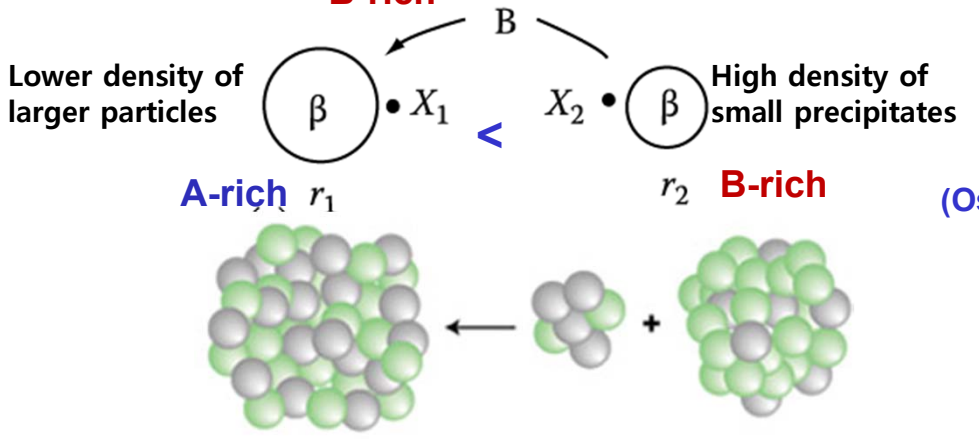

Assumption: volume diffusion is the rate controlling factor

$$\left(\bar{r}\right)^3 - r_0^{\,3} = kt$$

Average radius

where $k \propto D\gamma X_e$

(X_e: Equil. solubility of very large particles)

Coarsening rate $\dfrac{d\bar{r}}{dt} \propto \dfrac{k}{\bar{r}^2}$

(D and X_e ~ exp (-Q/RT) ⇨ CR ↑
$\bar{r}$
Rapidly increase with Increasing temp.

(Ostwald Ripening)

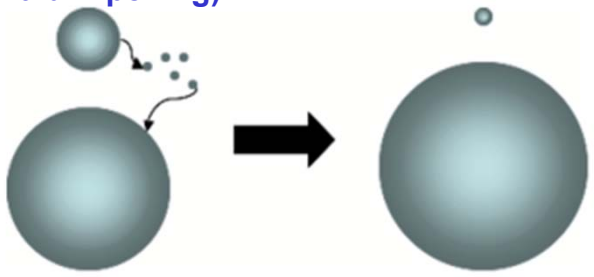

: Concentration gradient in matrix→diffusion→small particle_shrink/ large particle_grow

5.5.6. Particle Coarsening

The Rate of Coarsening with Increasing Time and Temp.

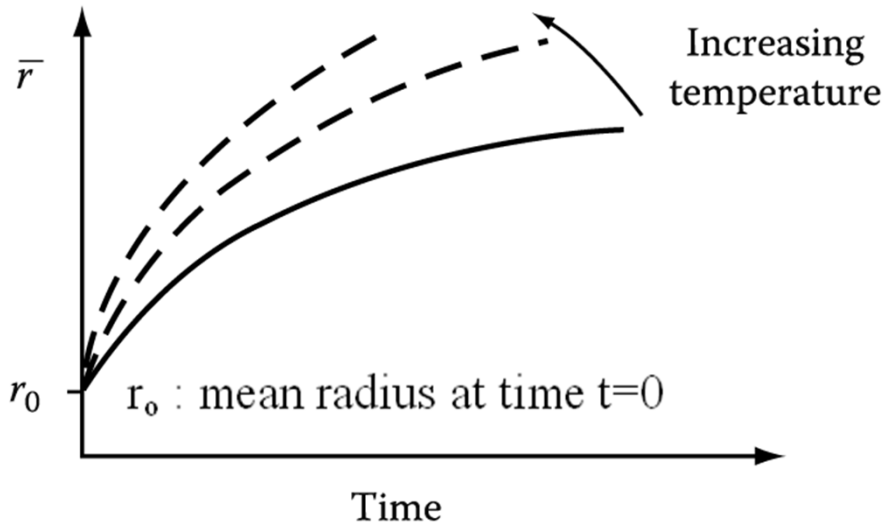

$\bar{r}$ ~ Particular concern in the design of materials for high temperature applications

Undesirable degradation of properties:
less strength/ disappearance of GB pinning effects

How can you design an alloy with high strength at high T?

→ **fine precipitate dispersion**

hint) $\frac{d\bar{r}}{dt} \propto \frac{k}{\bar{r}^2}$ $\quad k \propto D\gamma X_e$

1) low γ

heat-resistant Nimonic alloys

based on Ni-rich Ni-Cr → ordered fcc

$Ni_3(Ti,Al)$ in Ni-rich matrix → high strength

Ni/γ' interface~ "fully coherent" (10 ~ 30 mJ m^{-2})

Maintain a fine structure at high temperature

→ improve creep-rupture life

2) low X_e (Oxide~ very insoluble in metals)

: fine oxide dispersion in a metal matrix

Ex) dispersed fine ThO_2 (thoria) in W and Ni

→ strengthened for high temperature

3) low *D*

Cementite dispersions in tempered steel

→ high *D* of carbon → very quickly coarsening

a. substitutional alloying element

→ segregates to carbide → slow coarsening

b. strong carbide-forming elements

→ more stable carbides → lower X_e

Q7: Precipitation of Ferrite from Austenite ($\gamma \rightarrow \alpha$)

5.6. The Precipitation of Ferrite from Austenite (γ→α)

(Most important nucleation site: Grain boundary and the surface of inclusions)

The Iron-Carbon Phase Diagram

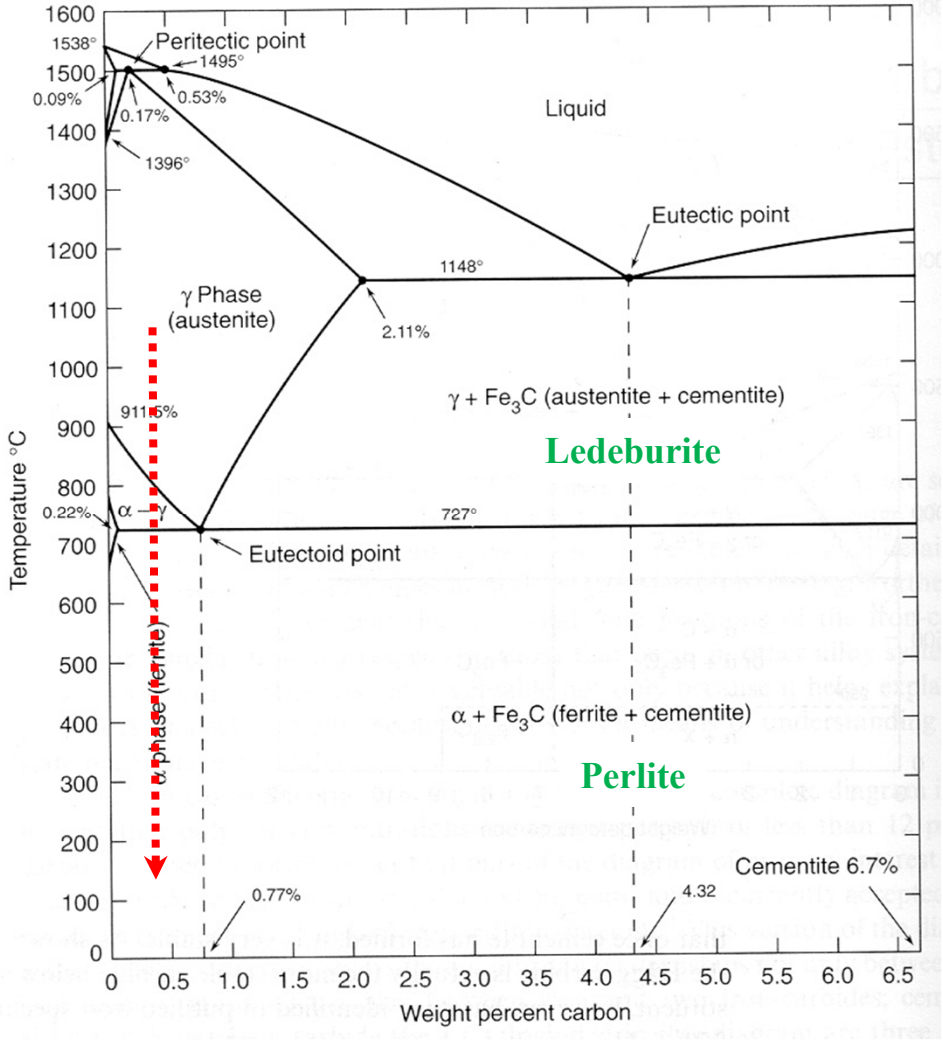

Microstructure (0.4 wt%C) evolved by slow cooling (air, furnace) ?

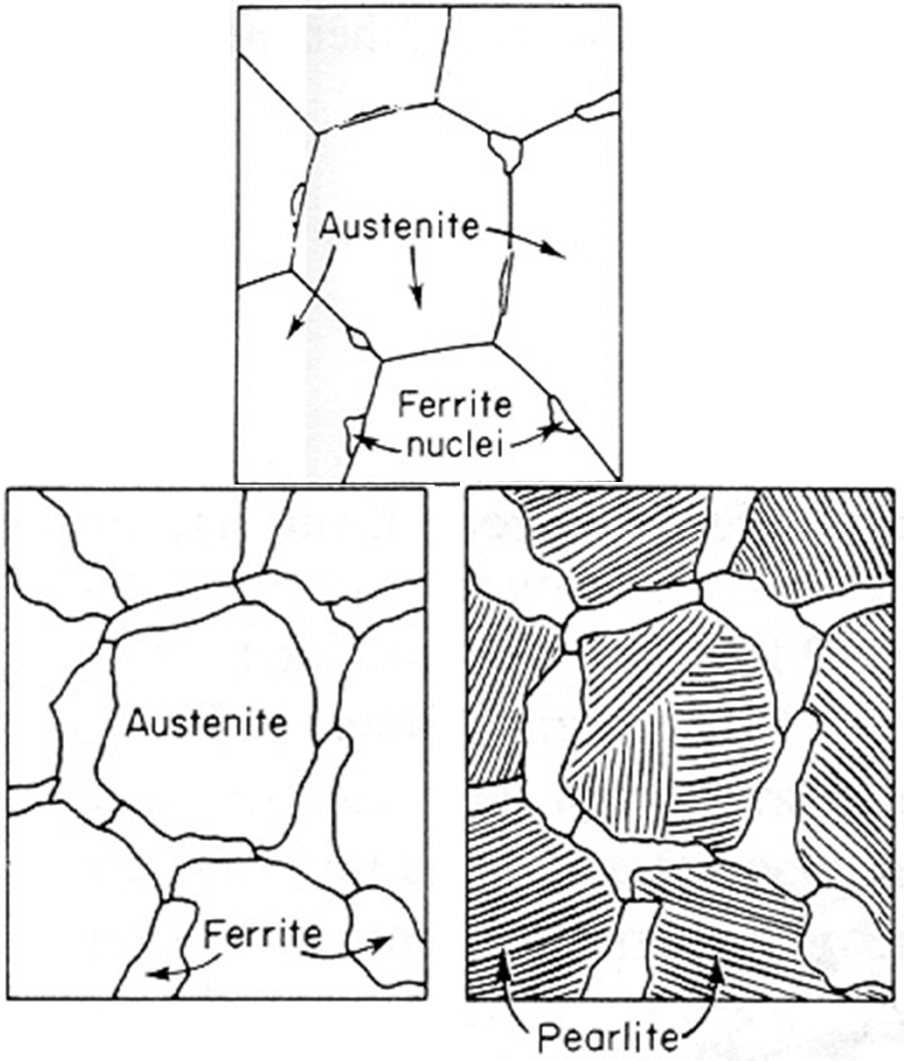

5.6. The Precipitation of Ferrite from Austenite

Diffusional Transformation of Austenite into Ferrite

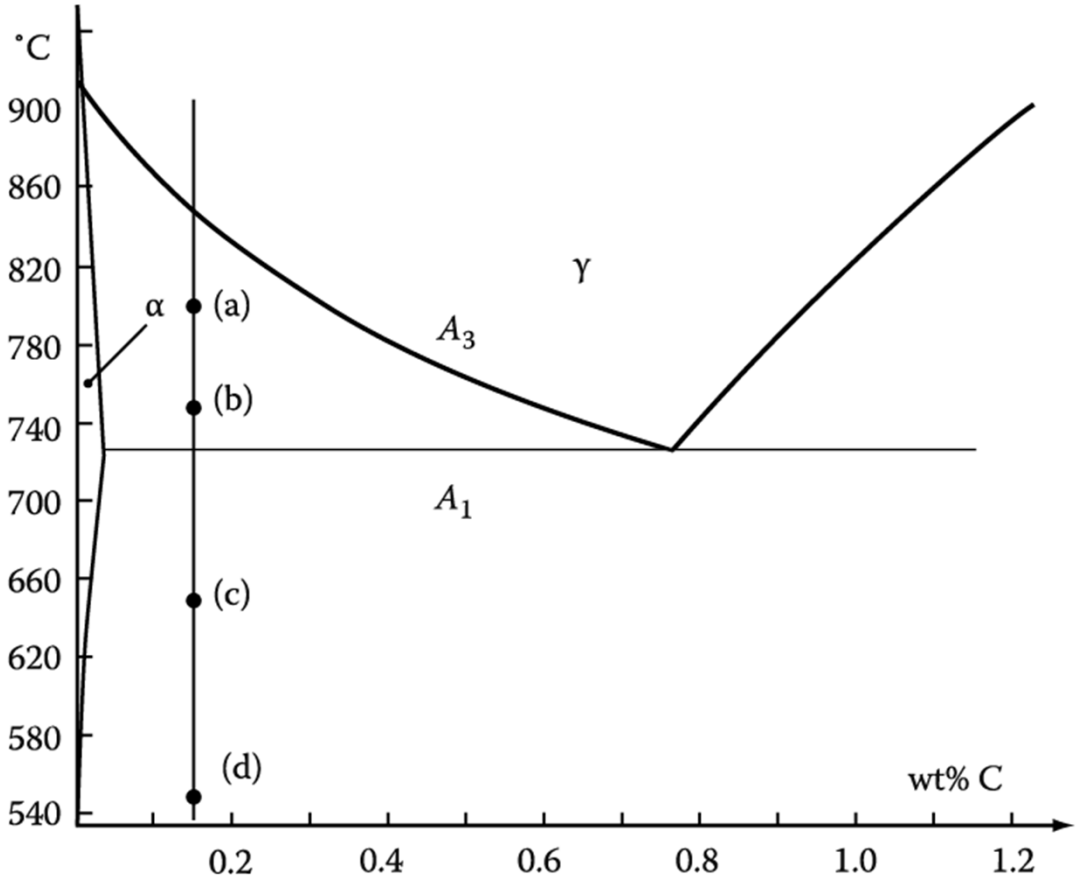

Figure 5.45 Holding temperature for steel in Figure. 5.46

Fe-0.15 wt%C

After being austenitized, held at

(a) 800°C for 150 s

(b) 750°C for 40 s

(c) 650°C for 9 s

(d) 550°C for 2 s and

then quenched to room T.

What would be the microstructures?

Microstructures of an austenitized Fe-0.15%C alloy (x 100 except (d, x300))

White: α ferrite/ Gray: M formed from untransformed γ/ fine constituent: a mixture of ferrite and carbide

Primary ferrite allotriomorphs with a few plates ⇨ Many more plates, mostly growing from GBs/ inside α grain

Smaller ΔT

(a)
800°C
for 150 s

(입계타형) G.B. allotriomorphs
"blockey" manner/
Smoothly curved & faceted α/γ
Interface are present

(b)
750°C
for 40 s

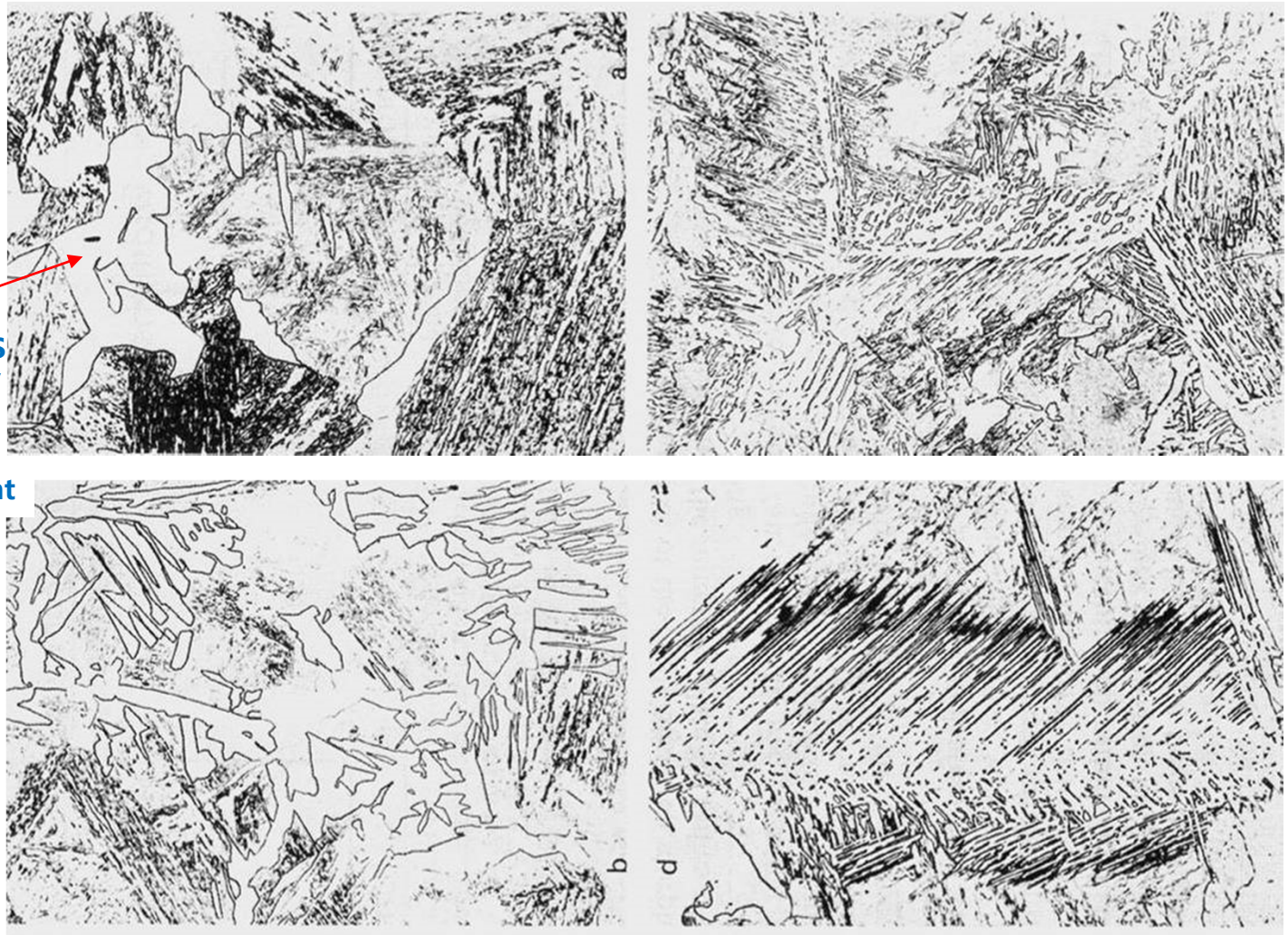

(c)
650°C
for 9 s

(d)
550°C
for 2 s

larger ΔT

Widmanstätten ferrite side-plates (b), (c), (d) _ Finer & faceted coherent interface with increasing "undercooling"

* Grain boundary allotriomorph 입계타형

Grain boundary precipitation → **Faster than allowed by volume diffusion**
involves three steps

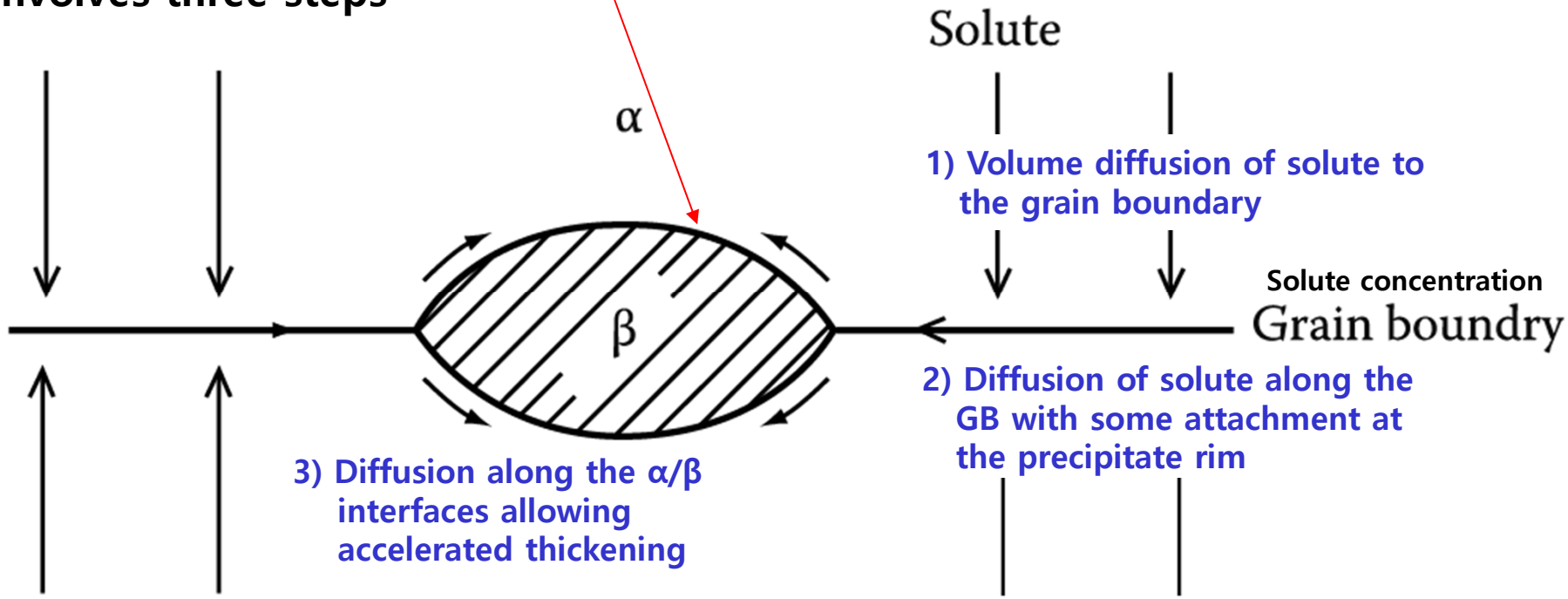

치환형 확산이 일어나는 경우 매우 중요/ 침입형 고용체에서는 체적 확산 속도가 크기 때문에 입계나 전위를 통한 단거리 확산은 상대적으로 중요하지 않음.

Fig. 5.18 Grain-boundary diffusion can lead to rapid lengthening and thickening of grain boundary precipitates, especially by substitutional diffusion.

The reason for the transition from grain boundary allotriomorphs to Widman -stätten side-plates with increasing undercooling is not fully understood.

→ possible answer: **Relative Velocity of Incoherent & Semicoherent Interfaces vary with undercooling**

a) At small undercoolings, both semi-coherent and incoherent interfaces ~similar rates

b) At large undercoolings, only incoherent interfaces~full use of increased driving force

(Continuous growth)

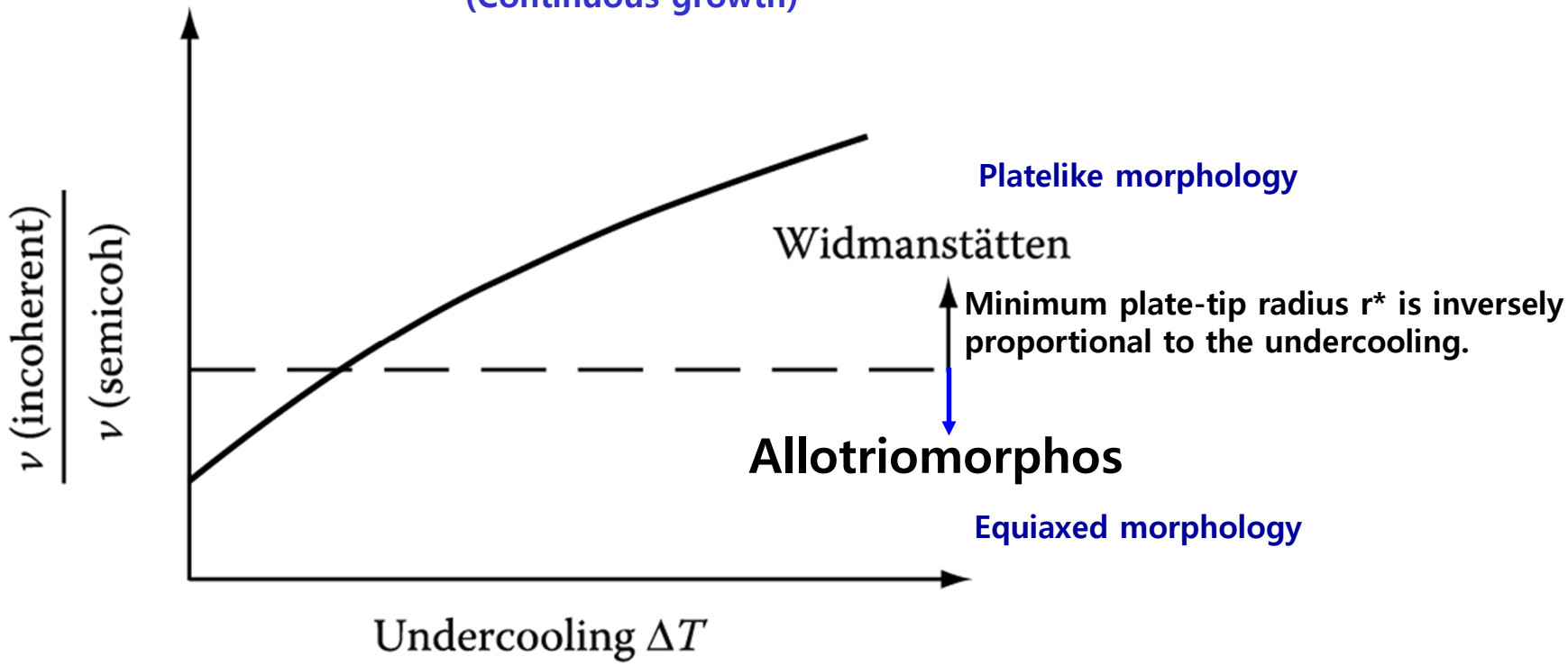

* Intragranular ferrite in large-grained specimen

: ferrite can also precipitate within the austenite grains (Fig. in page 17)
suitable heterogeneous nucleation site~inclusions and dislocations
generally equiaxed at low undercooling ↔ more platelike at higher undercolings

5.6. The Precipitation of Ferrite from Austenite

Typical TTT curve for $\gamma \rightarrow \alpha$ transformation $\rightarrow f(t,T)$

J-M-A Eq. $f = 1 - \exp(-kt^n)$

$-\frac{\pi}{3} Iv^3$

k: sensitive with T ***f*(*I*, *v*)**

n: 1 ~ 4 **(depend on nucleation mechanism)**

a) Time for a given percentage transformation will decrease as the constant *k* increase
b) *k* increases with increases in ΔT or total # of nucleation sites

→ Thus, decreasing the austenite grain size has the effect of shifting the C curve to shorter transformation times.

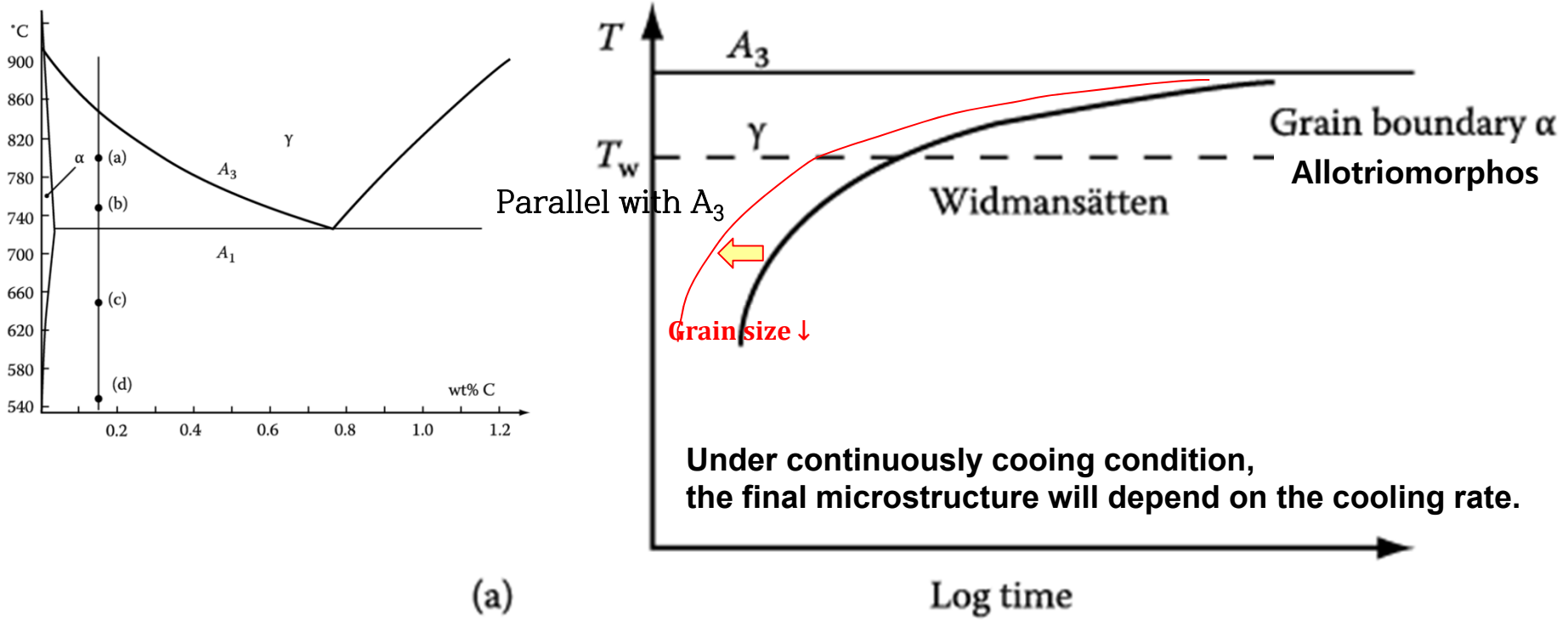

Figure 5.48 (a) typical TTT curve for $\gamma \rightarrow \alpha$ transformation in a hypoeutectoid steel: a typical C shape.

For alloys of different carbon content, A_3 and T_w vary and show parallel manner each other.

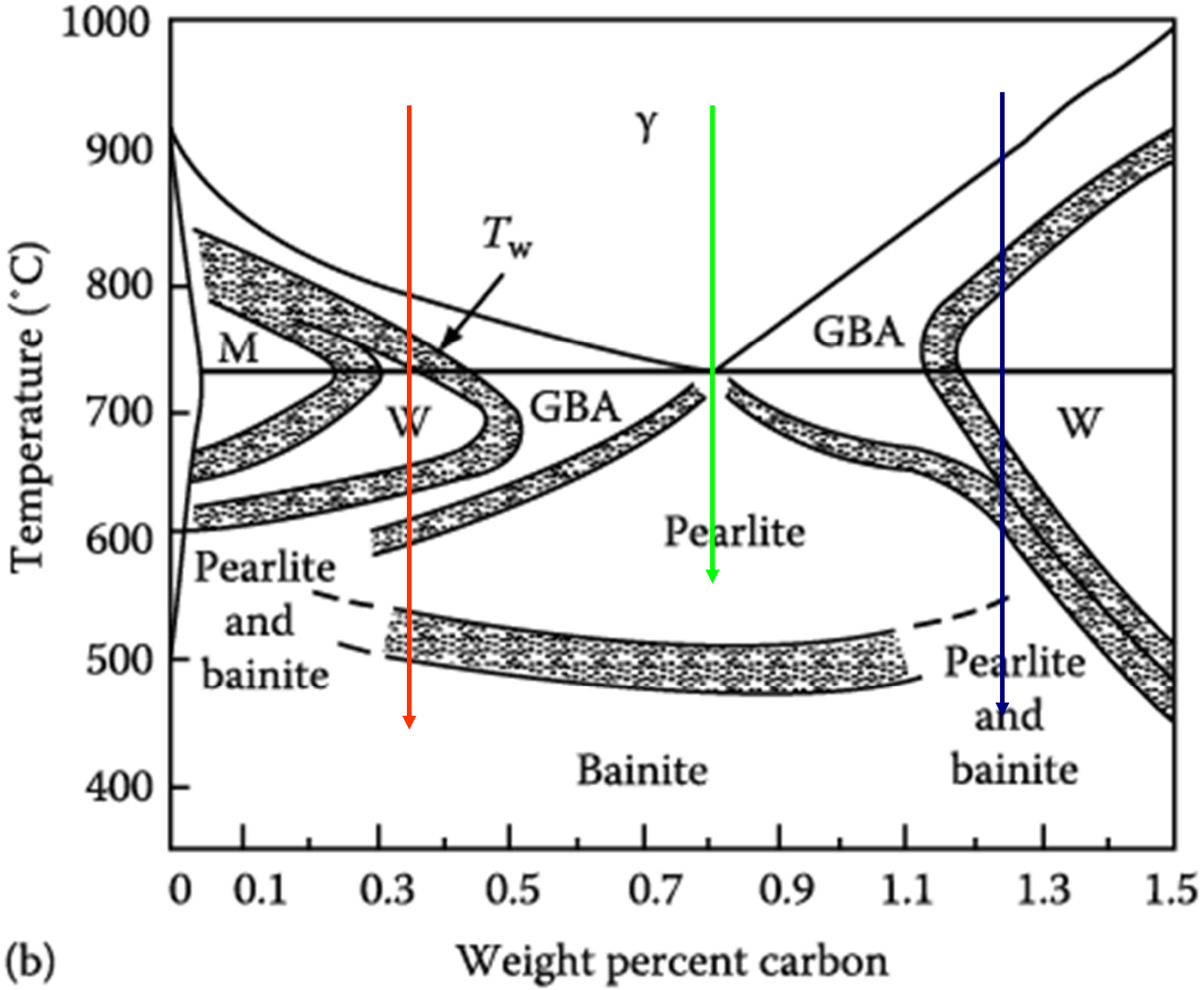

(GBA: GB allotriomorphs, W: Widmanstatten sideplates/intermolecular plates, M: Massive ferrite)

Figure 5.48 (b) Temperature-composition regions in which the various morphologies are dominant at late reaction times in specimens with ASTM grain size Nos. 0-1.

5.6.1 & 5.7 skip

5. Diffusion Transformations in solid

: diffusional nucleation & growth

(a) Precipitation

$$\alpha' \rightarrow \alpha + \beta$$

Metastable supersaturated
Solid solution

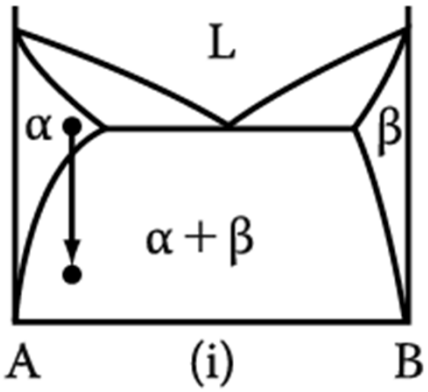

Homogeneous Nucleation

$$\Delta G = -V\Delta G_V + A\gamma + V\Delta G_S$$

$$N_{hom} = \omega C_0 \exp\left(-\frac{\Delta G_m}{kT}\right)\exp\left(-\frac{\Delta G^*}{kT}\right)$$

Heterogeneous Nucleation

$$\Delta G_{het} = -V(\Delta G_V - \Delta G_S) + A\gamma - \Delta G_d$$

➡ suitable nucleation sites ~ nonequilibrium defects
(creation of nucleus~destruction of a defect($-\Delta G_d$))

(b) Eutectoid Transformation

Composition of product phases differs from that of a parent phase.

→ **long-range diffusion**